

# Consensus clustering for Bayesian mixture models: Supplementary materials

Stephen Coleman, Paul DW Kirk and Chris Wallace

November 26, 2020

## Abstract

Description of models used and analyses performed.

## 1 Definitions

**Definition 1 (Consensus matrix)** *Given  $S$  clusterings for a dataset of  $N$  items,  $c_s = (c_{s1}, \dots, c_{sN})$ , the Consensus matrix is a  $N \times N$  matrix where the  $(i, j)^{th}$  entry records the proportions of clusterings for which items  $i$  and  $j$  are allocated the same label. More formally, it is the matrix  $\mathbb{C}$  such that*

$$\mathbb{C}(i, j) = \frac{1}{S} \sum_{s=1}^S \mathbf{I}(c_{si} = c_{sj}) \quad (1)$$

where  $\mathbb{I}(\cdot)$  is the indicator function taking a value of 1 if the argument is true and 0 otherwise.

**Definition 2 (Posterior similarity matrix)** *A Consensus matrix for which all the clusterings are generated from a converged Markov chain for some Bayesian clustering model. Sometimes abbreviated to PSM.*

**Definition 3 (Partition or Clustering)** *For a dataset of items  $X = (x_1, \dots, x_N)$ , a partition or clustering is a set of disjoint sets covering  $X$ , normally indicated by a  $N$ -vector of integers indicating which set each item is associated with. Note that these labels only have meaning relative to each other, they are symbolic. Each set within the clustering is referred to as a cluster.*

## 2 The models

### 2.1 Individual dataset

In the simulations (see section 4) where individual datasets are modelled a *Bayesian mixture model* is used. We write the basic mixture model for inde-

pendent items  $X = (x_1, \dots, x_N)$  as

$$x_n \sim \sum_{k=1}^K \pi_k f(x_n | \theta_k) \quad \text{independently for } n = 1, \dots, N \quad (2)$$

where  $f(\cdot | \theta)$  is some family of densities parametrised by  $\theta$ . A common choice is the Gaussian density function, with  $\theta = (\mu, \sigma^2)$  (as in our simulation study).  $K$ , the number of subgroups in the population,  $\{\theta_k\}_{k=1}^K$ , the component parameters, and  $\pi = (\pi_1, \dots, \pi_K)$ , the component weights are the objects to be inferred. In the context of *clustering*, such a model arises due to the belief that the population from which the random sample under analysis has been drawn consists of  $K$  unknown groups proportional to  $\pi$ . In this setting it is natural to include a latent *allocation variable*,  $c = (c_1, \dots, c_N)$ , to indicate which group each item is drawn from, with each non-empty component of the mixture corresponds to a cluster. The model is

$$\begin{aligned} p(c_n = k) &= \pi_k \quad \text{for } k = 1, \dots, K, \\ x_n | c_n \sim f(x_n | \theta_k) &\quad \text{independently for } n = 1, \dots, N. \end{aligned} \quad (3)$$

The joint model can then be written

$$p(X, c, K, \pi, \theta) = p(X|c, \pi, K, \theta)p(\theta|c, \pi, K)p(c|\pi, K)p(\pi|K)p(K)$$

We assume conditional independence between certain parameters such that the model reduces to

$$p(X, c, \theta, \pi, K) = p(\pi|K)p(\theta|K)p(K) \prod_{n=1}^N p(x_n | c_n, \theta_{c_n})p(c_n | \pi, K). \quad (4)$$

Additional flexibility is provided by the inclusion of hyperparameters on the priors for  $\pi$  and  $\theta$ , denoted  $\alpha$  and  $\eta$  respectively. In our context where  $\theta = (\mu, \sigma^2)$ , we use

$$\sigma^2 \sim \Gamma^{-1}(a, b), \quad (5)$$

$$\mu \sim \mathcal{N}(\xi, \frac{1}{\lambda} \sigma^2), \quad (6)$$

$$\pi \sim \text{Dirichlet}(\alpha). \quad (7)$$

The directed acyclic graph (**DAG**) for this model is shown in figure 1. The value of the hyperparameters we use are

$$\alpha = 1, \quad (8)$$

$$\xi = 0.0, \quad (9)$$

$$\lambda = 1.0, \quad (10)$$

$$a = 2.0, \quad (11)$$

$$b = 2.0. \quad (12)$$

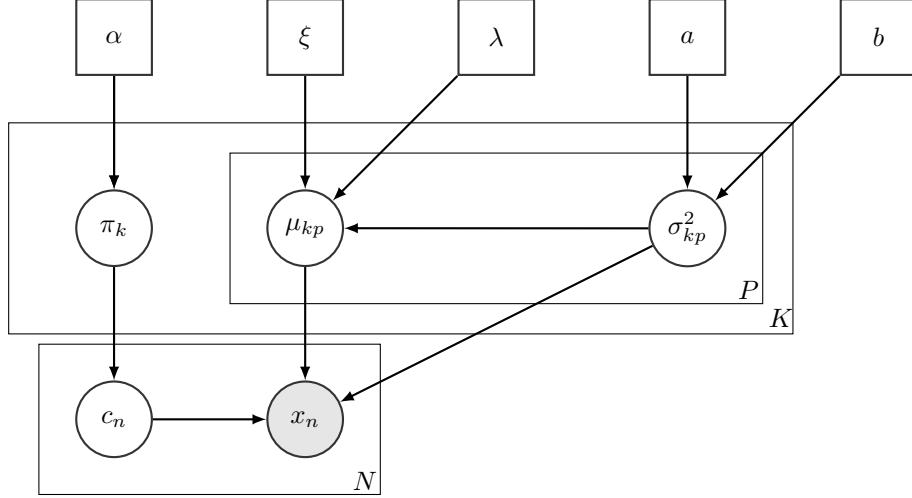


Figure 1: Directed acyclic graph for the mixture of Gaussians used.

## 2.2 Integrative clustering

We are interested in the use of Consensus clustering for integrative methods. We used Multiple Dataset Integration (**MDI**, Kirk et al., 2012) as an example of a Bayesian integrative clustering method. MDI models dataset specific clusterings, in contrast to, for example, Clusternomics (Gabasova et al., 2017) in which a *global clustering* is inferred.

The defining aspect of MDI is the prior on the allocation of the  $n^{th}$  item across the  $L$  datasets

$$p(c_{n1}, \dots, c_{nL}) \propto \prod_{l=1}^L \pi_{c_{nl}l} \prod_{l=1}^{L-1} \prod_{m=l+1}^L (1 + \phi_{lm} \mathbb{I}(c_{nl} = c_{nm})) \text{ for } n = 1, \dots, N. \quad (13)$$

$\phi_{lm}$  is the parameter defined by the similarity of the clusterings for the  $l^{th}$  and  $m^{th}$  datasets and is also sampled in each iteration. As  $\phi_{lm}$  increases more mass is placed on the common partition for these datasets. Conversely, in the limit  $\phi_{lm} \rightarrow 0$  we have independent mixture models. In other words, MDI allows datasets with similar clustering of the items to inform the clustering in each other more strongly than the clustering for an unrelated dataset. The DAG for this model for three datasets is shown in figure 2.

## 3 Consensus clustering

Consensus clustering is an ensemble approach to cluster analysis. Ensembles are often better able to explore the full parameter space than any individual

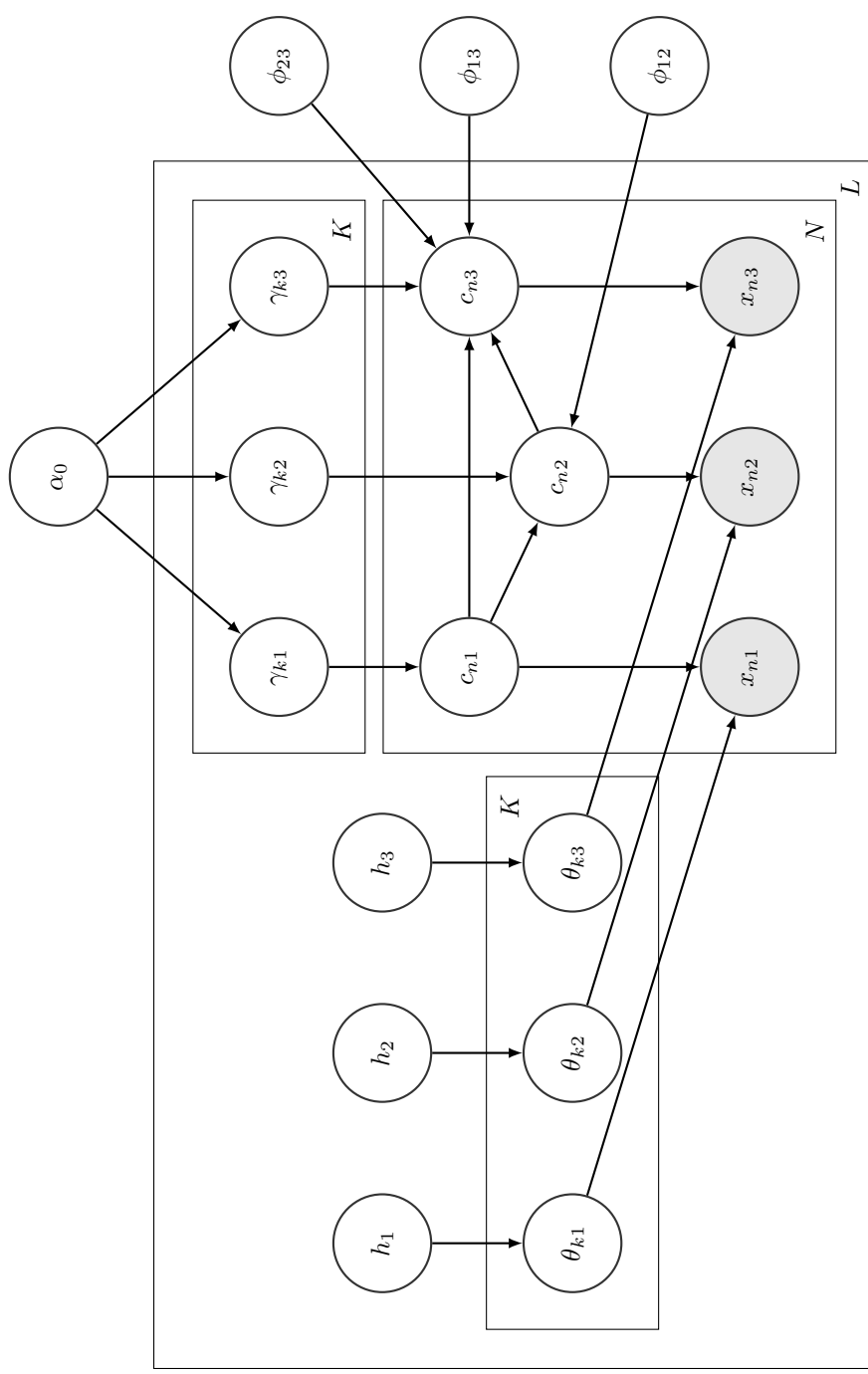


Figure 2: Directed acyclic graph for the Multiple Dataset Integration model for  $L = 3$  datasets.  $h_l$  is the choice of hyperpriors for the  $l^{th}$  dataset.

learner in its composition, thus describing more modes within parameters than the individual learners (Ghaemi et al., 2011). Ensembles also offer reductions in computational runtime because most ensemble methods enable use of a parallel environment to improve computation speed (Ghaemi et al., 2009).

Consensus clustering (Monti et al., 2003) is an ensemble method for cluster analysis, previously implemented using  $k$ -means clustering as the base learner in the R package **ConsensusClusterPlus** (Wilkerson et al., 2010). Consensus clustering has been applied in a variety of biomedical setting such as cancer subtyping (Lehmann et al., 2011; Verhaak et al., 2010), identifying subclones in single cell analysis (Kiselev et al., 2017), and proteomic characterisation of tumours (Xu et al., 2020). Consensus clustering applies  $S$  independent runs of the underlying clustering algorithm to perturbed versions of the dataset and combines the  $S$  final partitions in a *Consensus matrix* which is used to infer a final clustering. An outline of this is described in algorithm 1.

The consensus matrix is a symmetric matrix with the  $(i, j)^{th}$  entry being the proportions of model runs for which the  $i^{th}$  and  $j^{th}$  items are clustered together. For a single partition the *coclustering matrix* represents this information, being a binary matrix with the  $(i, j)^{th}$  entry indicating if items  $i$  and  $j$  are allocated to the same cluster.

```

Data:  $X = (x_1, \dots, x_N)$ 
Input: A resampling scheme Resample
A clustering algorithm Cluster
Number of resampling iterations  $S$ 
Set of cluster numbers to try  $\mathcal{K} = \{K_1, \dots, K_{max}\}$ 
Output: A predicted clustering,  $\hat{Y}$ 
The predicted number of clusters present  $\hat{K}$ 
begin
  for  $K \in \mathcal{K}$  do
    /* initialise an empty Consensus Matrix */  

     $\mathbf{M}^{(K)} \leftarrow \mathbf{0}_{N \times N};$   

    for  $s = 1$  to  $S$  do
       $X^{(s)} \leftarrow \text{Resample}(X);$   

      /* Cluster the perturbed dataset, represented in a  

       coclustering matrix */  

       $\mathbf{B}^{(s)} \leftarrow \text{Cluster}(X^{(s)}, K);$   

       $\mathbf{M}^{(K)} \leftarrow \mathbf{M}^{(K)} + \mathbf{B}^{(s)};$ 
    end
     $\mathbf{M}^{(K)} \leftarrow \frac{1}{S} \mathbf{M}^{(K)};$ 
  end
   $\hat{K} \leftarrow \text{best } K \in \mathcal{K} \text{ based upon all } \mathbf{M}^{(K)};$ 
   $\hat{Y} \leftarrow \text{partition } X \text{ based upon } \mathbf{M}^{(\hat{K})};$ 
end
```

**Algorithm 1:** Consensus Clustering algorithm

Ensemble methods are rarely applied Bayesian models despite Monti et al. (2003) suggesting this. We believe that Bayesian methods are underexploited in the ensemble framework and propose applying Consensus clustering to Bayesian mixture models. Our implementation of this is described in algorithm 2.

```

Data:  $X = (x_1, \dots, x_N)$ 
Input: A Bayesian mixture model with membership vector
 $c = (c_1, \dots, c_N)$ 
A clustering algorithm that generates samples  $Cluster$ 
The number of chains to run,  $S$ 
The number of iterations within each chain,  $R$ 
Output: A predicted clustering,  $\hat{Y}$ 
The consensus matrix  $M$ 
begin
    /* initialise an empty Consensus Matrix */  

     $M \leftarrow \mathbf{0}_{N \times N};$   

    for  $s = 1$  to  $S$  do  

        /* set the random seed controlling initialisation and  

         MCMC moves */  

         $set.seed(s);$   

        /* initialise a random partition on  $X$  drawn from the  

         prior distribution */  

         $Y_{(0,s)} \leftarrow Initialise(X);$   

        for  $r = 1$  to  $R$  do  

            /* generate a markov chain for the membership  

             vector */  

             $Y_{(r,s)} \leftarrow Cluster(c, r);$   

        end  

        /* create a coclustering matrix from the  $R^{th}$  sample */  

         $B^{(s)} \leftarrow Y_{(R,s)};$   

         $M \leftarrow M + B^{(s)};$   

    end  

     $M \leftarrow \frac{1}{S}M;$   

     $\hat{Y} \leftarrow \text{partition } X \text{ based upon } M;$ 
end

```

**Algorithm 2:** Consensus clustering for Bayesian mixture models

We show via simulation that ensembles consisting of short chains are sufficient to uncover meaningful structure in a number of scenarios including some within which a Gibbs sampler becomes trapped in individual modes for any reasonable length of runtime. The chains are both short and independent, thus their individual runtime is far shorter than the chains traditionally used for Bayesian inference and may also be run in parallel. This means that Consensus clustering of Bayesian mixture models offers significant reductions in runtime without sacrifices in performance. As the ensemble can describe multiple modes,

the uncertainty present in the consensus matrix can be more representative of the data than the individual modes captured by any single chain.

We then considered the multiple dataset setting. We applied Consensus clustering to an integrative extension of Bayesian mixture models, Multiple Dataset Integration (MDI). We applied this ensemble to three 'omics datasets for *Saccharomyces cerevisiae* and uncovered clusters that have a biological interpretation. We then compared this result to performing Bayesian inference of MDI.

### 3.1 Stopping rule for ensemble growth

As our ensemble sidesteps the problem of convergence within each chain, we need an alternative stopping rule for growing the ensemble in chain depth,  $R$ , and number of chains,  $S$ . We propose a heuristic based upon the Consensus matrix to decide if a given value of  $R$  and  $S$  are sufficient. We suspect that increasing  $S$  and  $R$  might continuously improve the performance of the ensemble, but we believe that these improvements will become smaller and smaller for greater values, approaching some asymptote for each of  $S$  and  $R$ .

Following this logic if the Consensus matrices for three ensembles define by the parameters  $(aR, S)$ ,  $(R, bS)$  and  $(R, S)$  are not visibly different for some reasonable values of  $a, b, S$  and  $R$  than increasing ensemble size or depth will see at most marginal improvement in performance. We suggest bounds of  $a, b \in (0, 0.5]$  and  $R \geq 100, S \geq 50$ , but make the general observation that large  $S$  and  $R$  are always better and that the closer  $a$  and  $b$  are to 0 the more strict the stopping criteria become.

A more interpretable visualisation is inspired by the logic of using a scree plot in Principal Component Analysis to decide the number of components to keep. Analogously to Consensus clustering where some improvement might always be expected for increasing chain length or number, more variance will always be captured by increasing the number of components used. However, again similarly to Consensus clustering, increasing this number beyond a certain point has diminishing returns. We recommend a plot of the mean squared difference between the Consensus matrices for a set of values of  $R' = \{r_1, \dots, r_I\}$  and  $S' = \{s_1, \dots, s_J\}$  to that for  $(r_I, s_J)$  (i.e. the Consensus matrix for  $\max(R')$  and  $\max(S')$ ). An example of this is included in the analysis of the yeast data in figure 15. If the values are no longer dropping sharply (i.e. the partial derivative of the mean squared difference with respect to  $R$  and  $S$  is small) than the change in the analysis for greater values of  $R$  or  $S$  is probably marginal.

If this heuristic is used, we believe that the Consensus matrix and the resulting inference should be stable. In contrast, if there is still strong variation in the Consensus matrix for varying chain length or number, than we believe that the inferred clustering is influenced significantly by the random initialisation. This means that the inferred partition that it is unlikely to be stable for similar datasets or reproducible for a random choice of seeds. This stability is often a desirous property in a clustering method (Von Luxburg and Ben-David, 2005; Meinshausen and Bühlmann, 2010).

## 4 Simulations

We defined a number of scenarios to test certain concepts of the method and to explore behaviour due to specific characteristics of real data. The parameters associated with each scenario in table 1 were used to generate individual simulations using algorithm 3. We compared Consensus clustering of Bayesian mixture models, a Bayesian inference of these models and **Mclust**, an implementation of mixture models that uses the maximum-likelihood estimator and an initialisation based upon hierarchical clustering.

Scenario	$N$	$P_s$	$P_n$	$K$	$\Delta\mu$	$\sigma^2$	$\pi$
2D	100	2	0	5	3.0	1	$(\frac{1}{5}, \frac{1}{5}, \frac{1}{5}, \frac{1}{5}, \frac{1}{5})$
No structure	100	0	2	1	0.0	1	1
Base Case	200	20	0	5	1.0	1	$(\frac{1}{5}, \frac{1}{5}, \frac{1}{5}, \frac{1}{5}, \frac{1}{5})$
Large standard deviation	200	20	0	5	1.0	9	$(\frac{1}{5}, \frac{1}{5}, \frac{1}{5}, \frac{1}{5}, \frac{1}{5})$
Large standard deviation	200	20	0	5	1.0	25	$(\frac{1}{5}, \frac{1}{5}, \frac{1}{5}, \frac{1}{5}, \frac{1}{5})$
Irrelevant features	200	20	10	5	1.0	1	$(\frac{1}{5}, \frac{1}{5}, \frac{1}{5}, \frac{1}{5}, \frac{1}{5})$
Irrelevant features	200	20	20	5	1.0	1	$(\frac{1}{5}, \frac{1}{5}, \frac{1}{5}, \frac{1}{5}, \frac{1}{5})$
Irrelevant features	200	20	100	5	1.0	1	$(\frac{1}{5}, \frac{1}{5}, \frac{1}{5}, \frac{1}{5}, \frac{1}{5})$
Varying proportions	200	20	0	5	1.0	1	$(\frac{1}{2}, \frac{1}{4}, \frac{1}{8}, \frac{1}{16}, \frac{1}{16})$
Varying proportions	200	20	0	5	0.4	1	$(\frac{1}{2}, \frac{1}{4}, \frac{1}{8}, \frac{1}{16}, \frac{1}{16})$
Small $N$ , large $P$	50	500	0	5	1.0	1	$(\frac{1}{5}, \frac{1}{5}, \frac{1}{5}, \frac{1}{5}, \frac{1}{5})$
Small $N$ , large $P$	50	500	0	5	0.2	1	$(\frac{1}{5}, \frac{1}{5}, \frac{1}{5}, \frac{1}{5}, \frac{1}{5})$

Table 1: Parameters defining the simulation scenarios as used in generating data and labels.

- *2D*: a low dimensional scenario within which we expected **Mclust** to perform well and the long chains to converge and explore the full support of the posterior distribution.
- *No structure*: we included this scenario to reassure fears that Consensus clustering has a predilection to finding clusters where none exist (Şenbabaoğlu et al., 2014a,b).
- *Base case*: highly informative datasets within which we expected methods to find the true generating labels quite easily. We included this scenario to benchmark the others that are variations of this setting.
- *Large standard deviation*: these two scenarios investigated the degree of distinction required between clusters for the methods to uncover their structure.
- *Irrelevant features*: we included these scenarios to investigate how robust the methods are to irrelevant features.

**Algorithm:** Simulation generation

**Input:** Distance between means  $\Delta_\mu$   
A common standard deviation  $\sigma^2$   
A number of clusters  $K$   
The number of items to generate in total  $N$   
The number of features to generate in total  $P$   
An indicator vector of feature relevance  $\phi = (\phi_1, \dots, \phi_P)$   
The expected proportion of items in each cluster  $\pi = (\pi_1, \dots, \pi_K)$   
A method for sampling  $x$  times from the array  $y$ , with weights  $\pi$ :  
 $Sample(y, x, \pi)$   
A method for permuting a vector  $x$ :  $Permute(x)$   
A method for generating a value from a univariate Gaussian  
distribution with mean  $\mu$  and standard deviation  $\sigma^2$ :  $Gaussian(\mu, \sigma^2)$

**Output:** A dataset,  $X$

The generating cluster labels  $c = (c_1, \dots, c_N)$

```

begin
    /* initialise the empty data matrix */ 
     $X \leftarrow 0_{N \times P};$ 
    /* create a matrix of  $K$  means */ 
     $\mu \leftarrow (\Delta_\mu, \dots, K\Delta_\mu);$ 
    /* generate the allocation vector */ 
     $c \leftarrow Sample(1 : K, N, \pi);$ 
     $M \leftarrow 0_{N \times N};$ 
    for  $p = 1$  to  $P$  do
        /* Test if the feature is relevant, if relevant
           generate data from a mixture of univariate
           Gaussians, otherwise draw all items from the same
           distribution */ 
        if  $\phi_p = 1$  then
             $\nu \leftarrow Permute(\mu);$ 
            for  $n = 1$  to  $N$  do
                |  $X(n, p) \leftarrow Gaussian(\nu_{c_n}, \sigma^2)$ 
            end
        end
        if  $\phi_p = 0$  then
            for  $n = 1$  to  $N$  do
                |  $X(n, p) \leftarrow Gaussian(0, \sigma^2)$ 
            end
        end
    end
    /* Mean centre and scale the data */ 
     $X \leftarrow Normalise(X)$ 
end

```

**Algorithm 3:** Data generation for a mixture of Gaussian with independent features. This algorithm is implemented in the `generateSimulationDataset` function from the `mdiHelpR` package available at [www.github.com/stcolema mdiHelpR](http://www.github.com/stcolema mdiHelpR).

- *Varying proportions*: these scenarios investigated how well each method uncovers clusters when the clusters have significantly different membership counts.
- *Small  $N$ , large  $P$* : an investigation of behaviour when the number of features is far greater than the number of items.

#### 4.1 Bayesian analysis

For each simulation we ran 10 chains for 1 million iterations, keeping every thousandth sample. We discarded the first 10,000 iterations to account for burn-in bias, leaving 990 samples per chain. To check if the chains were converged we used

- the Geweke convergence diagnostic (Geweke et al., 1991) to investigate within-chain stationarity, and
- the potential scale reduction factor ( $\hat{R}$ , Gelman et al., 1992) and the Vats-Knudson extension (*stable*  $\hat{R}$ , Vats and Knudson, 2018) to check across-chain convergence.

The Geweke convergence diagnostic is a standard Z-score; it compares the sample mean of two sets of samples (in this case buckets of samples from the first half of the samples to the sample mean of the entire second half of samples). It is calculated under the assumption that the two parts of the chain are asymptotically independent and if this assumption holds (i.e. the chain is sampling the same distribution in both samples) then the scores are expected to be standard normally distributed. If a chain's Geweke convergence diagnostic passed a Shapiro-Wilks test for normality (Shapiro and Wilk, 1965) (based upon a threshold of 0.05), we considered it to have achieved stationarity and included it in the model performance analysis.

$\hat{R}$  is expected to approach 1.0 if the set of chains are converged. Low  $\hat{R}$  is not sufficient in itself to claim chain convergence, but values above 1.1 are clear evidence for a lack of convergence (Gelman et al., 2013). Vats and Knudson (2018) show that this threshold is significantly too high (1.01 being a better choice) and propose extensions to  $\hat{R}$  that enable a more formal rule for a threshold. We use their method as implemented in the R package `stableGR` (Knudson and Vats, 2020) as the final check of convergence. An example of the  $\hat{R}$  series across the 100 simulations for a scenario where chains are well-behaved is shown in figure 3.

We focused upon stationarity of the continuous variables as assessing convergence of the allocation labels is difficult due to label-switching. In our simulations the only recorded continuous variable is the concentration parameter of the Dirichlet distribution for the component weights.

We pooled the samples from the stationary chains and used these to form a PSM. This and the point estimate clustering found by applying the R function `maxpear` (Fritsch, 2012) to this PSM are used in model performance analysis

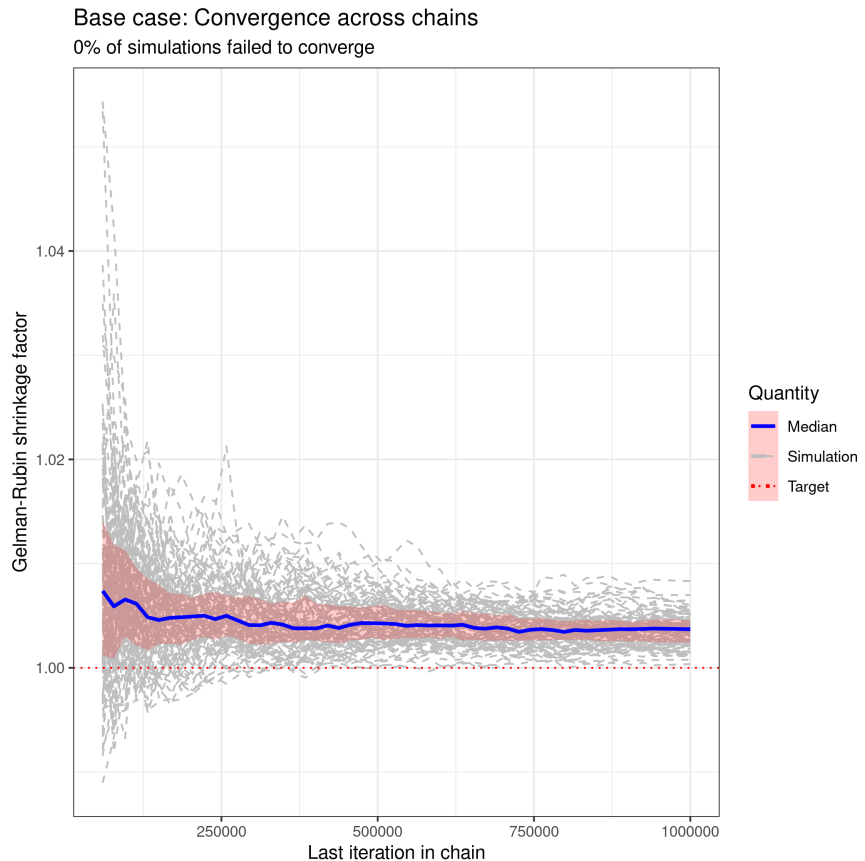


Figure 3: The  $\hat{R}$  values for each simulation (in dotted grey), the median value and the interquartile range across simulations. One can see that  $\hat{R}$  approaches 1.0, being below 1.01 for every simulation by the end of the chains. The “0% of simulations failed to converge” is a statement based upon the percentage of simulations which passed the test of stable  $\hat{R}$ .

in section 4.4. `maxpear` attempts to find the clustering that maximises the Adjusted Rand Index to the true clustering by using an approximation of the expected clustering under the posterior,  $\mathbb{E}(c|X)$ , believing that this converges to the true clustering. A sample average clustering is used to approximate the expected clustering. This is estimated from the PSM by maximising

$$\frac{\sum_{i < j} \mathbb{I}(c_i^* = c_j^*) p_{ij} - \sum_{i < j} \mathbb{I}(c_i^* = c_j^*) \sum_{i < j} p_{ij} / \binom{N}{2}}{\frac{1}{2} \left[ \sum_{i < j} \mathbb{I}(c_i^* = c_j^*) + \sum_{i < j} p_{ij} \right] - \sum_{i < j} \mathbb{I}(c_i^* = c_j^*) \sum_{i < j} p_{ij} / \binom{N}{2}} \quad (14)$$

where  $p_{ij}$  is the  $(i, j)^{th}$  entry of the PSM (Fritsch et al., 2009). When the chain has converged this maximises the posterior expected ARI to the true clustering.

There are three possibilities to consider the decision to pool the samples across chains under:

- The chains are converged and agree upon the distribution sampled (see figure 4 for an example).
- The chains are not in agreement upon the partition sampled, becoming trapped in different modes. However, a mode does dominate being the mode present in a majority of chains (see figure 5 for an example of this behaviour).
- The chains are not in agreement and no one mode dominates among chains (see figure 6 for an example of this behaviour).

In the first case pooling has no effect upon the predicted clustering compared to using any one chain. In the second case it feels natural that one would use the mode that dominates. Pooling the samples effectively does this for the predictive performance of the method as the mode with the greatest number of samples across the chains dominates; however, the uncertainty for this mode is increased. In the third case the analysis is non-trivial and further thought, chains and samples would be required. In our simulations this case only arises in the most pathological form in the second *Large N, small P* scenario, where each chain remains trapped in the initial partition. The clustering inferred from any chain is not meaningful being a random clustering; thus the clustering predicted by pooling the PSMs is no more or less relevant as it too is random.

## 4.2 Consensus clustering analysis

We investigated a range of ensembles, using all combinations of chain depth,  $R = (1, 10, 100, 1000, 10000)$ , and the number of chains,  $S = (1, 10, 30, 50, 100)$ . This gave a total of 25 different ensembles. A Consensus matrix was constructed from the samples generated by each ensemble by finding the proportion of samples within which any pair of items are coclustered. An example of the Consensus matrices for each ensemble in a given simulation is shown in figure 7. We used the `maxpear` function from the R package `mcclust` to create a point clustering estimate from the Consensus matrix. In this context where we do not assume



Figure 4: Posterior similarity matrices for the simulation generated using a random seed set to 1 for the first large standard deviation scenario from table 1. This is an example of all stationary chains agreeing in a simulation (and thus pooling of samples is no different to using any choice of chain for the performance analysis). Ordering of rows and columns is defined by hierarchical clustering of the first matrix in the series, in this case that from Chain 1.

### Small N large P ( $\Delta\mu = 1.0$ )

Posterior similarity matrices (simulation 1)

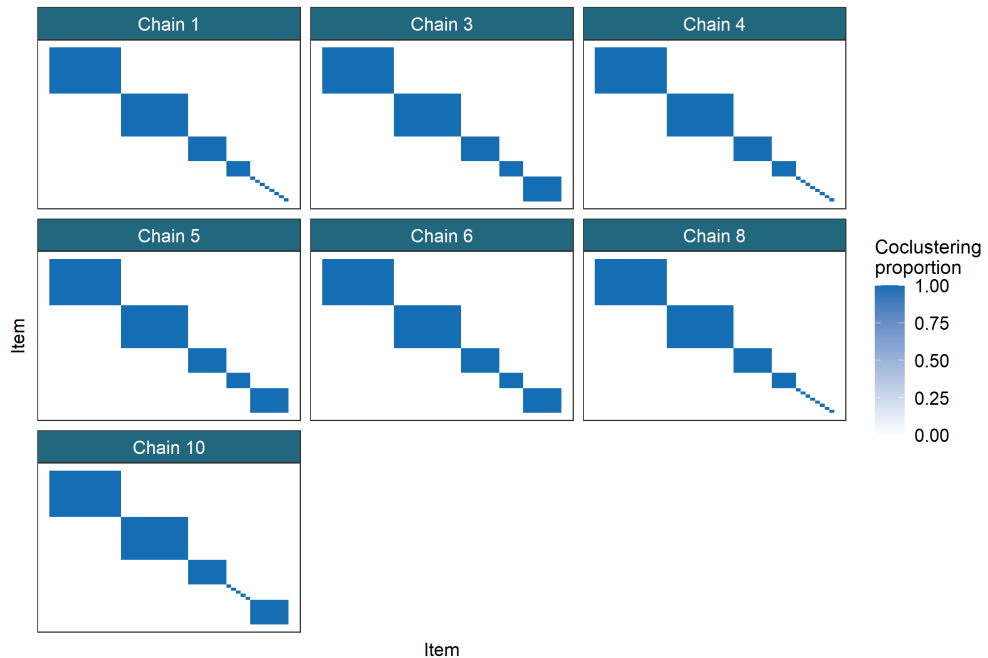


Figure 5: Posterior similarity matrices for the simulation generated using a random seed set to 1 for the first small  $N$ , large  $P$  scenario from table 1. This is an example of different chains becoming trapped in different modes, but one mode (which does represent the generating structure well) is dominant, being fully present in 3 of the 6 chains, with the two other modes present having significant overlap. Ordering of rows and columns is defined by hierarchical clustering of the first matrix in the series, in this case that from Chain 1.

### Small N large P ( $\Delta\mu = 0.2$ )

Posterior similarity matrices (simulation 1)

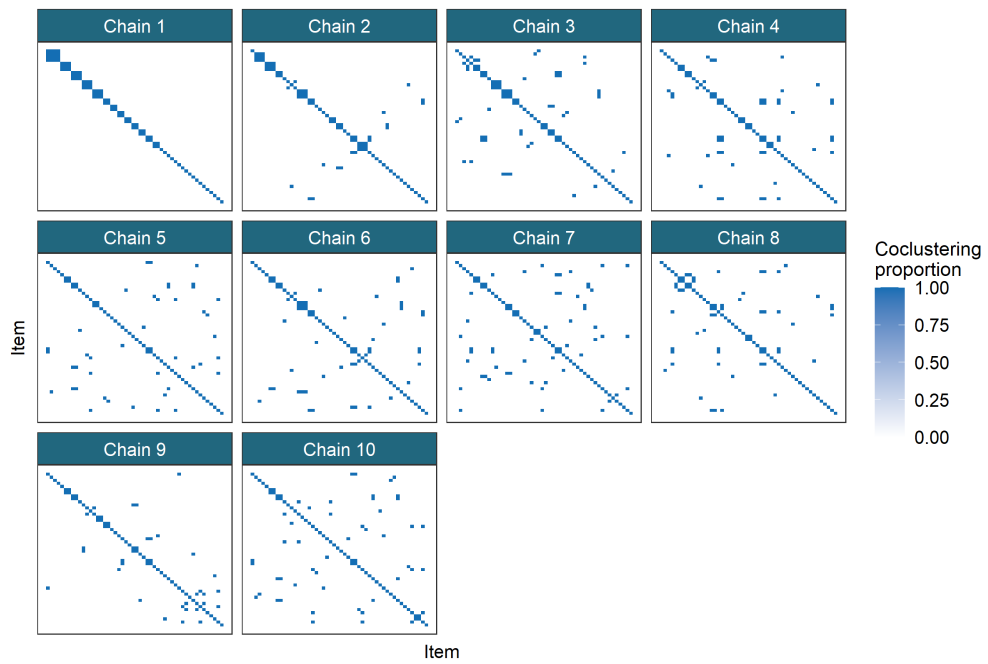


Figure 6: Posterior similarity matrices for the simulation generated using a random seed set to 1 for the second small  $N$ , large  $P$  scenario from table 1. This is an example of different chains becoming trapped in different modes with no mode being dominant. In this scenario each chain remains trapped in initialisation. Ordering of rows and columns is defined by hierarchical clustering of the first matrix in the series, in this case that from Chain 1.

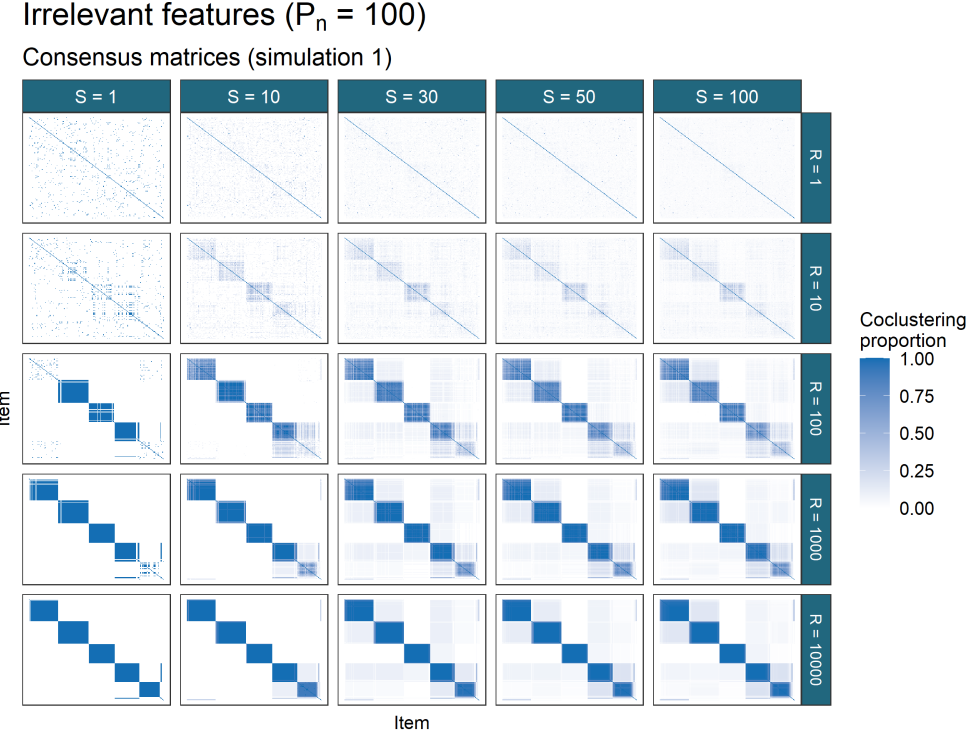


Figure 7: Consensus matrices for the simulation generated using a random seed set to 1 for the third irrelevant features scenario from table 1.  $R$  is the individual chain length and  $S$  is the number of chains used. In this example there are several modes present (as seen in the entries with values between 0 and 1) but one mode is clearly dominant (the 5 dark squares along the diagonal which correspond closely to the generating labels).

that the Consensus matrix of the samples is the Posterior similarity matrix we do not expect that the predicted clustering maximises the posterior expected ARI. Instead `maxpear` is used as calculating a sample average clustering which we believe is representative of the ensemble.

### 4.3 Mclust

We called `Mclust` using the default settings and a range of inputs for the choice of  $K$ . We used  $K = (2, \dots, \min(\frac{N}{2}, 50))$  to mirror the choice of  $K_{max} = 50$  used for the overfitted mixture models (the default in the software we used), with the bound of  $\frac{N}{2}$  to avoid fitting 50 clusters in the *Small N, large P* scenario where  $N = 50 = K_{max}$ . In the *No structure* scenarios we extended to range to  $K = (1, \dots, 50)$  to include the correct structure as an option. The model choice was performed using the Bayesian Information Criterion (Schwarz et al., 1978,

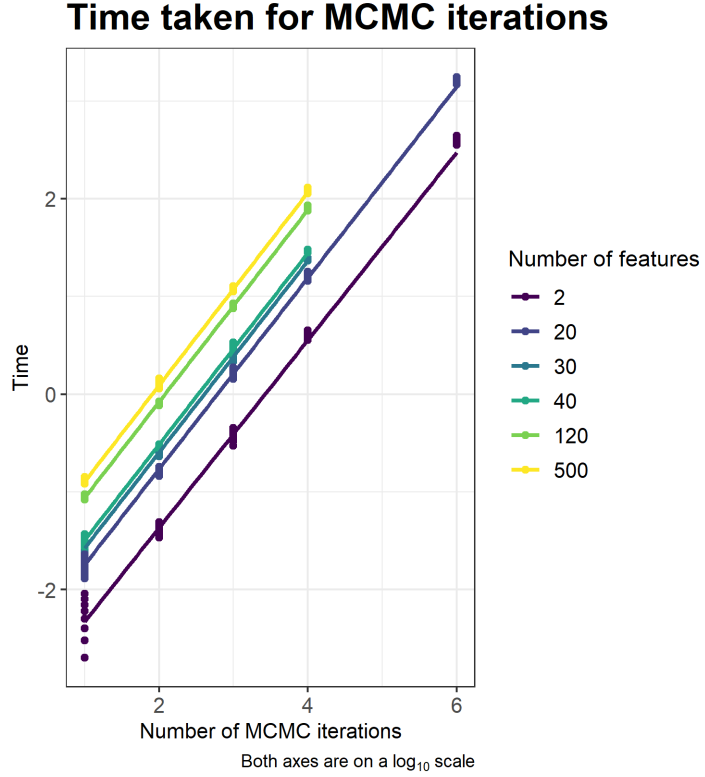


Figure 8: The time taken for different numbers of iterations of MCMC moves in  $\log(s)$ . The relationship between chain length,  $R$ , and the time taken is linear, with a change of intercept for different dimensions.

as implemented in `Mclust`). `Mclust` tries different covariance matrices and thus the model choice is not just between different values of  $K$ .

## 4.4 Model performance

### 4.4.1 Time

We measured the Bayesian chains to Consensus clustering using the terminal command `time`, measured in milliseconds. We compare these results in figure 8 and find that the gains in computation runtime achieved by Consensus clustering when a parallel environment is available can be enormous due to the shorter chains and independence between chains.

#### 4.4.2 Predictive performance

The different models (Bayesian (pooled), **Mclust** and the 25 Consensus clustering ensembles) were compared under their ability to predict the generating clustering and their uncertainty about this quantity.

In figure 12 the ARI between the generating labels and the point estimate clustering from each method is shown. For two partitions  $c_1, c_2$ ,

- $ARI(c_1, c_2) = 1.0$ : a perfect match between the two partitions,
- $ARI(c_1, c_2) = 0.0$ :  $c_1$  is no more similar to  $c_2$  than is expected for a random partition of the data.

In several scenarios **Mclust** performs the best under this metric (e.g. in the scenarios *2D, Small N, large P* ( $\Delta\mu = 0.2$ )). However when the number of irrelevant features is large **Mclust** performs less well (see *Irrelevant features* ( $P_n = 20$ ) and ( $P_n = 100$ )) than the other methods. In the scenario that  $P_n = 100$  failing to find structure is not inherently wrong as a majority of the features suggest that there are no subpopulations. We suspect that the initialisation based upon hierarchical clustering initialises the model in or very near to a small local mode in the likelihood surface and thus higher values of  $K$  are rejected as under the BIC as the model fit is not significantly improved and the model complexity is higher.

The pooled Bayesian samples act as an upper bound on the Consensus clustering ensembles in these simulations.

For the ensembles there are two parameters changing between each model, the iteration used to provide the clustering in the ensemble,  $R$ , and the number of chains (and hence samples) used,  $S$ . In many of the scenarios we find that the benefit of increasing  $R$  stabilises by approximately  $R = 10$ . We believe that in a low-dimensional dataset (such as *2D*), or a highly informative dataset (such as *Base case* or any of the higher dimensional scenarios with no irrelevant features where  $\frac{\Delta\mu}{\sigma^2} \geq 1$ ) the chains quickly find a “sensible” partition of the data and thus increasing the depth within the chain does not increase the probability that any partition sampled will be closer to the generating partition. For example in figure 12 in the *Small N, large P* case, the distribution of the ARI across the ensembles for which  $R \geq 10$  and  $S = 1$  is nearly identical; this suggests that the chain is sampling a very similar partition again and again for 9,990 iterations (and possibly beyond based upon the PSMs shown in figure 5) and it is through adding more chains rather than using particularly long chains that we improve the ability to uncover the generating structure.

We also notice that even if the behaviour has not stabilised for  $R$  that the ensemble can uncover meaningful structure. The ARI for the ensembles of short chains can be quite high (as is the case in many of the scenarios). The behaviour of the Consensus matrices also shows that low  $R$  is not a disqualifier from meaningful inference even if longer chains would be ideal, a result that might be useful in real applications with large datasets and complex models. Consider the Consensus matrices in figure 7, it can be seen that the behaviour has not stabilised

before  $R = 10000$  (and possibly there is still some benefit in increasing  $R$  beyond this value), but the structure being uncovered when there is a sufficient number of chains and  $R$  is small does correspond to the structure uncovered in the largest and deepest ensemble. We believe that the order in which components merge and items are co-clustered varies depending on initialisation, and thus if the chain is not sufficiently deep that all of the final mergings have occurred that a sufficiently large ensemble can still perform meaningful inference of the subpopulation structure despite the poor performance of any individual model. Even though each learner probably has too many clusters for small  $R$  the consensus among them will have less if the individual learners have low correlation between their partitions (something we might expect if the chains are stopped very early). This is why the entries of the Consensus matrix for  $R = 100$  and  $S = 100$  in figure 7 are more pale than in deeper ensembles; very few items correctly (possibly none) cocluster in every partition, it is only in observing the consensus that the global structure of interest emerges. Thus if there is some limit to the length of chains available for an analysis (e.g. computational or temporal constraints) than the inference obtained from the shorter chains can still be meaningful, with the caveat that the point clustering might have more clusters than the same analysis with longer chains would provide. Additional post-hoc merging of some clusters might be necessary in this case.

In contrast, when the dataset is sparse or contains many irrelevant features, we believe that deeper chains are required to reach this steady-state sampling where no single sample is expected to be better than any other (see the *Irrelevant features ( $P_n = 100$ )* facet of figure 12).

In some scenarios no method is successful in uncovering the generating labels. In the *Large standard deviation ( $\sigma^2 = 25$ )* and *Small  $N$ , large  $P$  ( $\Delta\mu = 0.2$ )* this is due to the lack of signal - the clusters overlap so significantly that it is not possible for any of these methods to uncover much of the generating structure. In the *No structure* case it is different (although *Mclust* does perform well here). In this case all items are generated from a common distributions. For the Bayesian chains and the ensembles, a clustering of singletons is predicted; each item is allocated a unique label (see figures 9 and 10). While failing to perform well under the ARI, this is a sensible result. Rather than indicating (as we did with the shared label) that no item is particularly distinct from the others and thus all share a common label, this clustering of singletons states that no item is more similar to any other and thus no two items should cluster together. It is an alternative statement of the same result, i.e. that there is no evidence for subpopulation structure. We consider this evidence that an ensemble of Bayesian mixture models is not as susceptible to predicting labels than an ensemble based upon  $K$ -means clustering as in Şenbabaoglu et al. (2014a,b).

Increasing  $S$  is also required when the dimensionality of the dataset is large. In this case it is due to individual chains exploring only a single mode (as can be seen in figure 5 where each chain appears to sample only a single partition). In this example where each sample is a partition that appears to be a mode in the posterior distribution of the allocation vector from very early in the chain

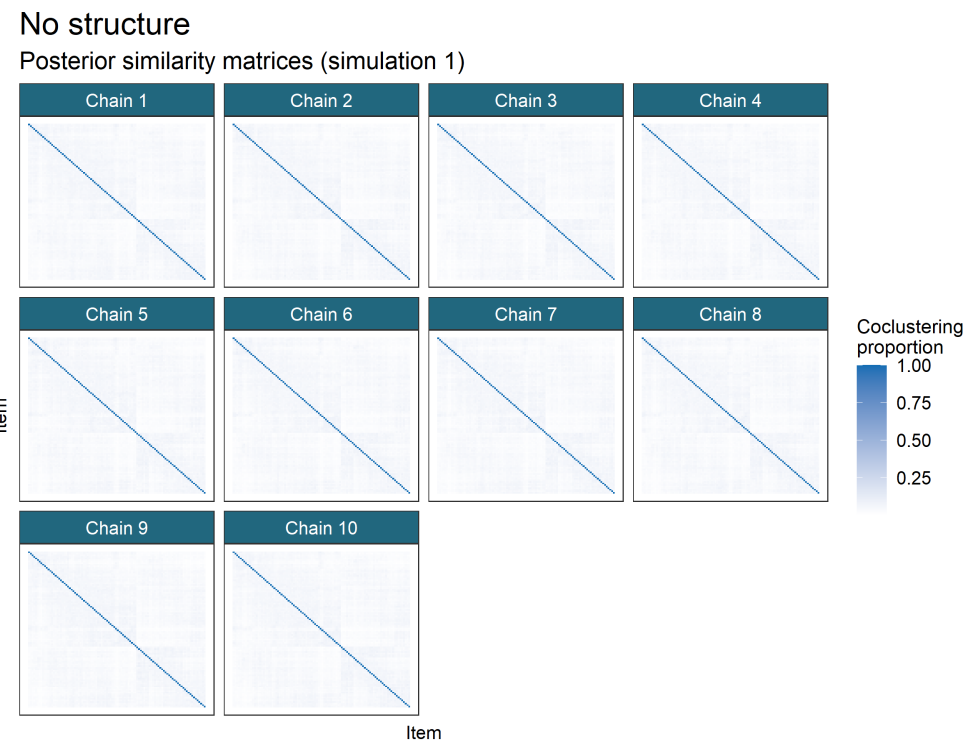


Figure 9: Posterior similarity matrices for simulation 1 of the *No structure* scenario. Each item is allocated to a singleton.

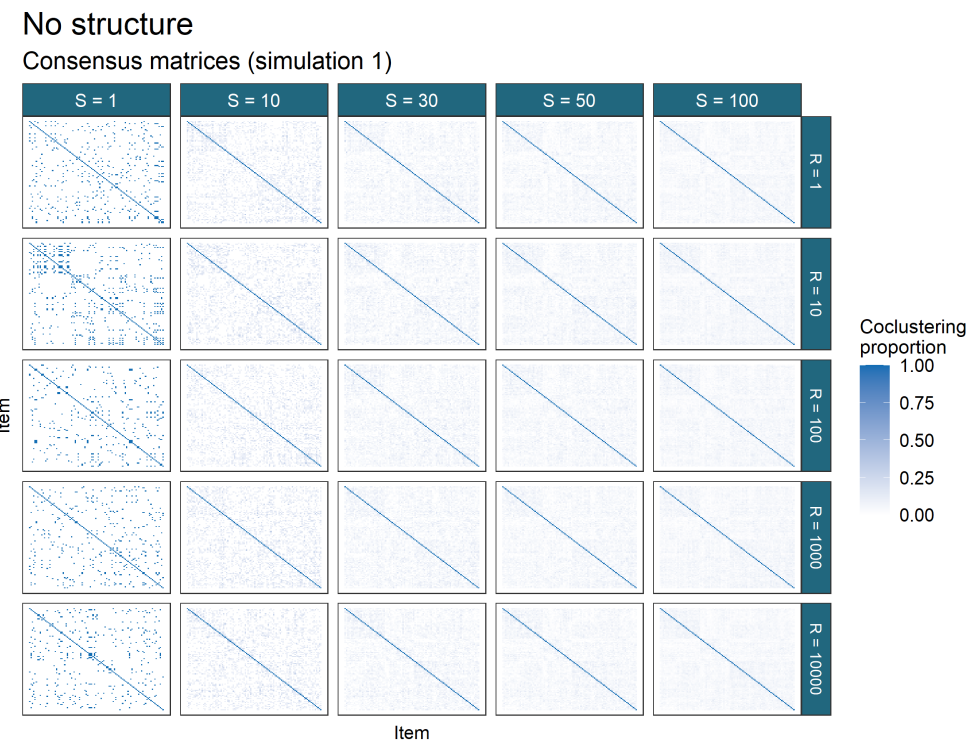


Figure 10: Consensus matrices for simulation 1 of the *No structure* scenario. Each item is allocated to a singleton in many of the Consensus matrices.

### Small N large P ( $\Delta\mu = 1.0$ )

Consensus matrices (simulation 1)

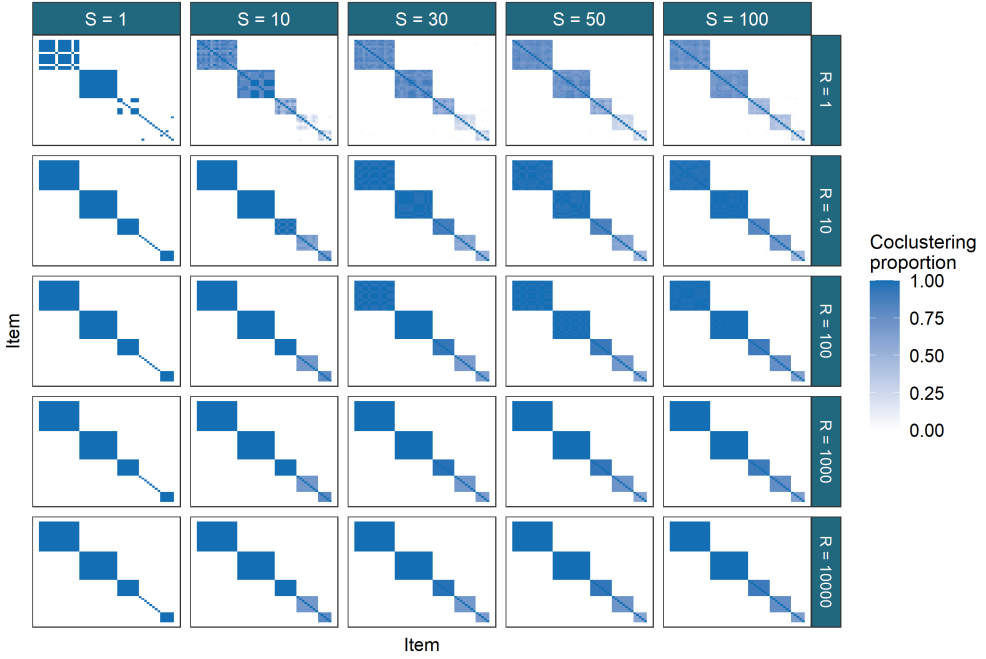


Figure 11: Consensus matrices for simulation 1 of the first *Large N, small P* scenario. One can see that by iteration ten the sample being drawn is from the mode (for  $S = 1, R = 10$ ), and that an ensemble of chains does find structure that recalls the generating labels (see figure 12, the ARI for  $CC(10, s)$  is 1.0 for  $s > 1$ , meaning that the true labels perfectly align with those predicted by the Consensus matrix).

(based upon the stable performance for  $R \geq 10$ ), increasing  $S$  allows each chain to “vote” on which mode is the global mode, as we believe that the mode that attracts the most chains is the global mode (although in real datasets the number of chains required might be greater than in our simulations). An example of this behaviour may be seen in figure 11.

In figure 12, limiting behaviour for increases of  $S$  and  $R$  can be seen for the ensemble. For most simulations there is no change in performance for greater choices of  $S$  and  $R$  after some stabilising values.

## 5 Yeast

The cell cycle is the process by which a growing cell divides into two daughter cells. This involves virtually all cellular processes - metabolism, protein syn-

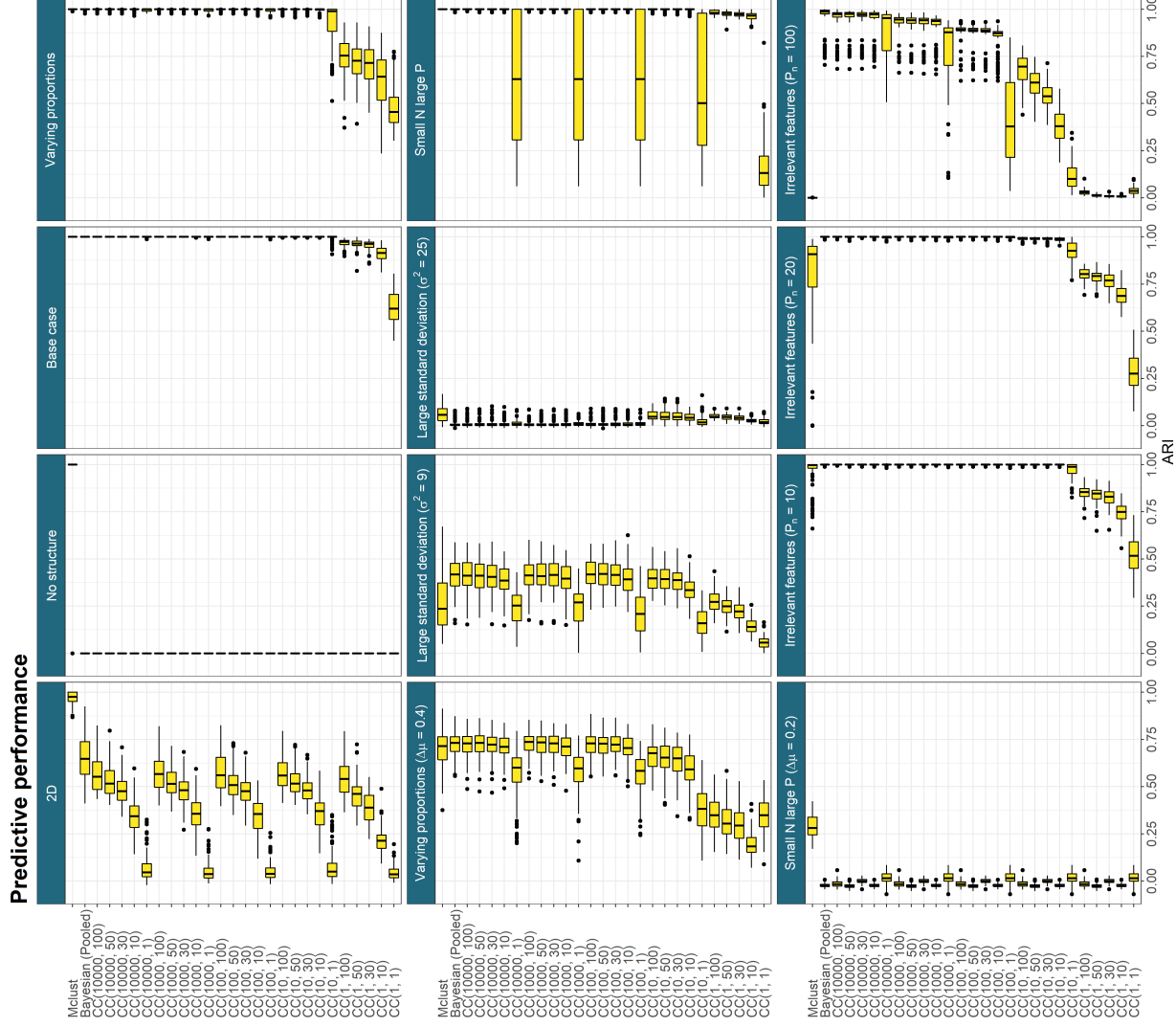


Figure 12: Predictive performance across all simulations.  $CC(R, S)$  denotes Consensus clustering using the  $R^{th}$  sample from  $S$  different chains. In the cases where the generating structure is not exactly found, increasing  $R$  and  $S$  sees some improvement in the ARI between the truth and the predicted clusterings before some limiting behaviour emerges and further increase appears to have no change in the performance.

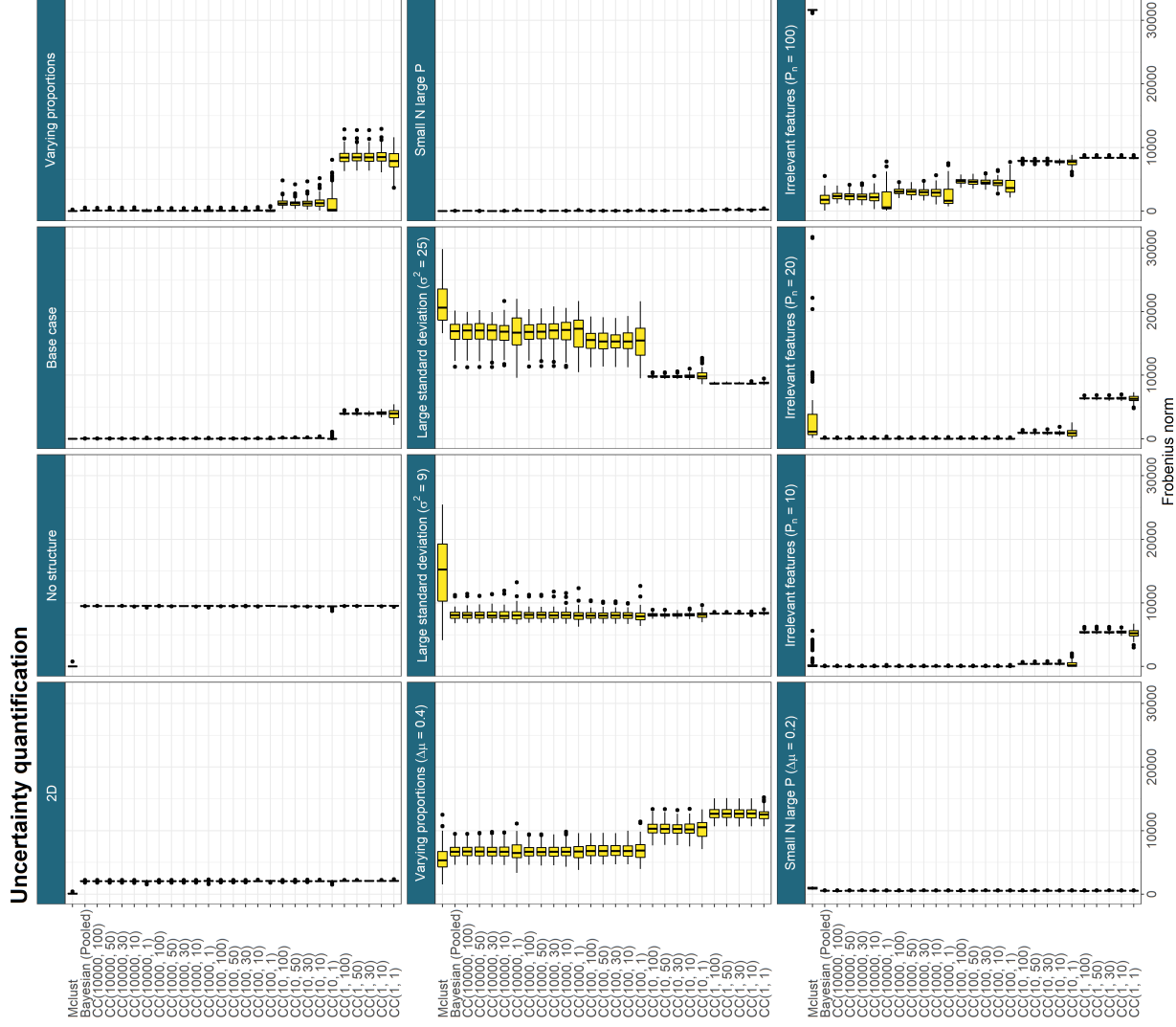


Figure 13: Frobenius norm across simulations.  $CC(R, S)$  denotes Consensus clustering using the  $R^{th}$  sample from  $S$  different chains. Lower values are better. In the *Large standard deviation ( $\sigma^2 = 25$ ) scenario, the very low valued entries from the ensembles of very short chains are rewarded. These ensembles are not closer to the true structure than the longer ensembles, but they are rewarded for the lack of certainty.*

thesis, secretion, DNA replication, organelle biogenesis, cytoskeletal dynamics and chromosome segregation - and diverse regulatory events (Granovskaia et al., 2010). The cell cycle is crucial to biological growth, repair, reproduction, and development; it is fundamental to sustaining life (Tyson et al., 2013; Chen et al., 2004; Alberts et al., 2018). The regulatory proteins of the system first appeared over a billion years ago and are so highly conserved among eukaryotes that many of them function perfectly when transferred from a human cell to a yeast cell (Alberts et al., 2018). This conservation means that a relatively simple eukaryote such as *Saccharomyces cerevisiae* can provide insight into a variety of cell cycle perturbations including those that occur in human cancer (Ingalls et al., 2007; Chen et al., 2004) and ageing (Jiménez et al., 2015). Budding yeast is particularly attractive for genetic analysis as it can proliferate as haploid cells, its genetic makeup can be easily altered by standard tools of molecular genetics, and large numbers of cells may be synchronised in a particular stage of the cell cycle (Tyson et al., 2013; Juanes, 2017).

To better understand the regulatory mechanisms and the genes most important in this process, we performed an integrative cluster analysis of gene products across three yeast datasets. These datasets were generated using different 'omics technologies and target different aspects of the molecular biology underpinning the cell cycle process.

- Microarray profiles of RNA expression from Granovskaia et al. (2010). This dataset comprises measurements of cell-cycle-regulated expression at 5-minute intervals for 41 time points (up to three cell division cycles) and is referred to as the **Timecourse** dataset. We include only the genes identified by Granovskaia et al. (2010) as having periodic expression profiles. This includes some non-coding RNAs (**ncRNAs**) of which the majority are anti-sense RNAs.
- Chromatin immunoprecipitation followed by microarray hybridization (**ChIP-chip**) data from Harbison et al. (2004). This dataset discretizes *p*-values from tests of association between 117 DNA-binding transcriptional regulators and a set of yeast genes. Based upon a significance threshold these *p*-values are represented as either a 0 (no interaction) or a 1 (an interaction).
- Protein-protein interaction (**PPI**) data from BioGrid (Stark et al., 2006). This database consists of physical and genetic interactions between gene and gene products. The interactions included are a collection of results observed in high throughput experiments and some computationally inferred interactions. The dataset we used contained 603 proteins as columns. An entry of 1 in the  $(i,j)^{th}$  cell indicates that the  $i^{th}$  gene has a protein product that is believed to interact with the  $j^{th}$  protein.

We used these datasets to construct sets of co-regulated genes that share biological functions in *Saccharomyces cerevisiae*. We believe such informed gene

sets are more relevant to phenotypic traits and offer insight into more complex biological processes.

We believe that the integrative aspect of the experiments means that the clusters are more interpretable than in a standalone cluster analysis. Cluster analysis of a single dataset entails interpreting the clusters defined by similarity within a single experiment which often involves strong assumptions about the biological processes behind the result (e.g. correlation of transcripts implies co-regulation).

We used the MDI model for our integrative analysis. This jointly models the clustering in each dataset, inferring individual clusterings for each dataset that are informed by similarity in the other clusterings. As described in section 2, MDI learns the similarity between the datasets being analysed and does not assume global structure. This means that the similarity between datasets is not strongly assumed in our model; individual clusters or genes that align across datasets are based solely upon the evidence present in the data not strong modelling assumptions. Thus we can include the PPI data and expect it to contribute to our final clustering despite the expectation that there will be less shared information between the Timecourse dataset with its large set of ncRNAs and this PPI dataset.

The datasets were reduced to 551 items by considering only the genes with no missing data in the PPI and ChIP-chip data. The choices to reduce the datasets to these 551 genes are the same steps as in Kirk et al. (2012). The datasets are shown in figure 14.

We used these datasets to perform an integrative analysis as many of the protein encoding genes in the mitotic cell cycle have well studied genomic binding sites with mapped transcription factors that control phase-specific expression (Cho et al., 1998; Spellman et al., 1998); thus the inclusion of the ChIP-chip data means that the clusters that align across the datasets should include well studied regulatory proteins and thus be of biological interest. If a cluster of genes are similarly expressed in the Timecourse, share associated regulatory protein in the ChIP-chip and are associated with common protein complexes in the PPI data, than this implies a gene set with strong biological significance.

In contrast, if we cluster the Timecourse dataset alone, any clusters that we find are defined by correlation across time. This might be assumed to be driven by shared regulatory mechanisms, but other sources of structure might be encouraging this, even experimental error. However, if a cluster aligns across both the Timecourse dataset and the ChIP-chip dataset we can be more certain that these genes are part of some regulatory network; if this cluster also emerges in the PPI dataset we might believe that the genes are co-regulated as part of the formation of some protein complex. Furthermore, this integrative aspect means that clusters that might merge in the Timecourse dataset due to similar periodicity in a standalone analysis might remain separate due to different associated transcription factors in the ChIP-chip dataset.

Thus we performed an integrative analysis using MDI to avoid aggressive assumptions about either the biology defining any clusters and modelling assumptions about the latent structure.

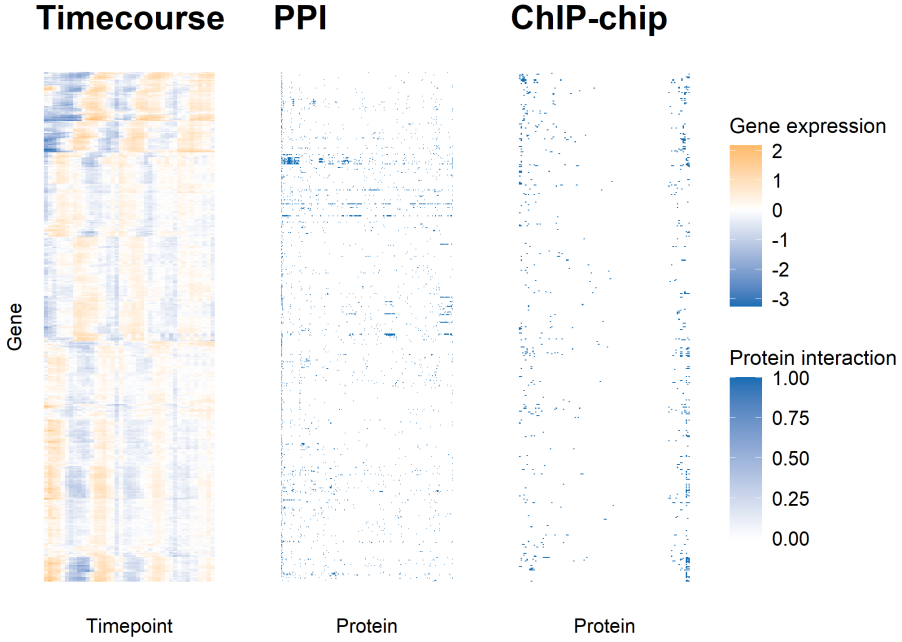


Figure 14: Heatmap of the yeast datasets. Each plot has a common row order corresponding to the gene products being clustered. This order was decided by a hierarchical clustering of the rows of the Timecourse expression matrix. The Timecourse data is associated with the “Gene expression” legend and the ChIP-chip and PPI data with “Protein interaction” legend.

We expect that the complexity of this data and model means that the time required for convergence of the MCMC algorithm would be very large. We avoid this problem by using Consensus clustering of MDI, instead basing our final ensemble choice on the stopping rule laid out in section 3.1.

The datasets were modelled using a mixture of Gaussian processes in the Timecourse dataset and Multinomial distributions in the ChIP-chip and PPI datasets. To ensure that our mixture model is initially overfitted we set  $K_{max} = 275 \approx \frac{N}{2}$ .

## 5.1 Consensus clustering analysis

### 5.1.1 Ensemble choice

We use an ensemble of depth  $R = 10001$  and width  $S = 1000$  with a base learner of MDI (using the software implementation from Mason et al., 2016). This ensemble depth and width were decided using the stopping rule from section 3.1. We include the Consensus matrices for this ensemble and those for

the combinations of  $R = (1001, 5001, 10001)$ ,  $S = (100, 500, 1, 000)$  in the three datasets (shown in figures 18, 19 and 20) and a plot of the mean squared difference between the Consensus matrix for  $R = 10001$  and  $S = 1000$  to a range of smaller and shallower ensembles (figure 15).

We decide to stop increasing at  $R = 10001$  as there is little change between Consensus matrices for increasing chain depth from  $R = 5001$  to  $R = 10001$  across the three datasets. An example of insufficient depth can be seen for  $R = 1001$  in figure 20; there is a marked difference in the Consensus matrices between  $R = 1001$  and  $R = 5001$ .

In terms of the number of chains required, we believe this to have stabilised, as there is no obvious change in increasing  $S$  from 100 in the Timecourse and ChIP-chip datasets, and none in any dataset for increasing from  $S = 500$  to  $S = 1000$ .

## 5.2 Cluster analysis

We use `maxpear` to infer an estimate clustering from the Consensus matrices as in the Simulations except we set `k.max = 275`.

### 5.2.1 Integrated genes

We wish to identify groups of genes that tend to be grouped together in multiple datasets. We use the concept of *fused genes* proposed by Savage et al. (2010) and used by Kirk et al. (2012), but to avoid confusion due to other possible ideas of fused genes (e.g. those that contribute to a common protein complex, the behaviour of TFs upon a gene) we use the term *integrated*. We define a gene to be integrated across some set of datasets if the gene has the same label in each of these datasets for at least half of the recorded clustering samples. Integrated genes are those most affected by the integrative aspect of the analysis and therefore we focus upon these in the following analysis. In our case we have the possible sets of:

- {Timecourse}, {ChIP-chip}, {PPI},
- {Timecourse, ChIP-chip}, {Timecourse, PPI}, {ChIP-chip, PPI}, and
- {Timecourse, ChIP-chip, PPI}.

Any set of a single dataset is the trivial case that all genes are considered integrated.

The number of integrated genes between any two datasets is indicative of how strongly they influence each other and is expected to align with the  $\phi_{lm}$  parameters from the MDI model. We find the following number of unique genes integrated between each combination of datasets:

- Timecourse + ChIP-chip + PPI: 56,
- Timecourse + ChIP-chip: 205 (261 including the 56 integrated across all datasets),

## Yeast data

Consensus clustering ensemble choice

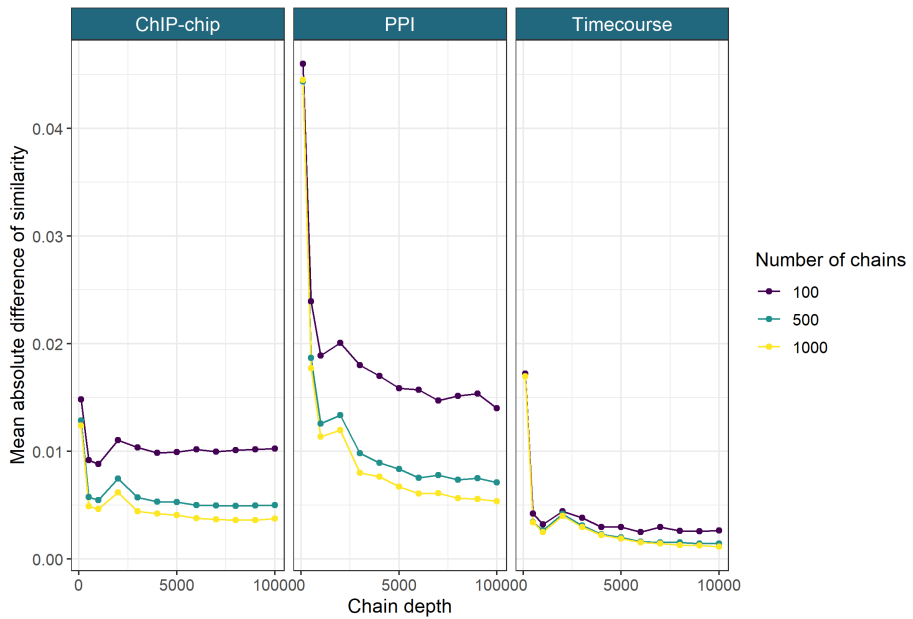


Figure 15: The mean squared difference between the sequential Consensus matrices for increasing chain depth  $r$  and  $s$  chains. For a set of chain lengths,  $R' = \{r_1, \dots, r_I\}$  and number of chains,  $S' = \{s_1, \dots, s_J\}$ , we take the sum of the squared difference between the Consensus matrix for  $(r_i, s_j)$  and  $(r_{i-1}, s_j)$  (here  $R' = \{101, 501, 1001, 2001, \dots, 10001\}$  and  $S' = \{100, 500, 1000\}$ ). We find that increasing  $s$  beyond 500 has marginal effect except in the PPI dataset. It appears that the improvement from increasing the ensemble depth and width is diminishing, with no strong improvement after  $R = 2,000$ . We include a horizontal line with a y intercept of 30.305 which corresponds to a change an average change in off-diagonal cell entries of 0.01 for  $N = 551$ . For each dataset this threshold is crossed for large  $r$  and  $s$ .

## Consensus clustering

Sampled  $\phi$  densities

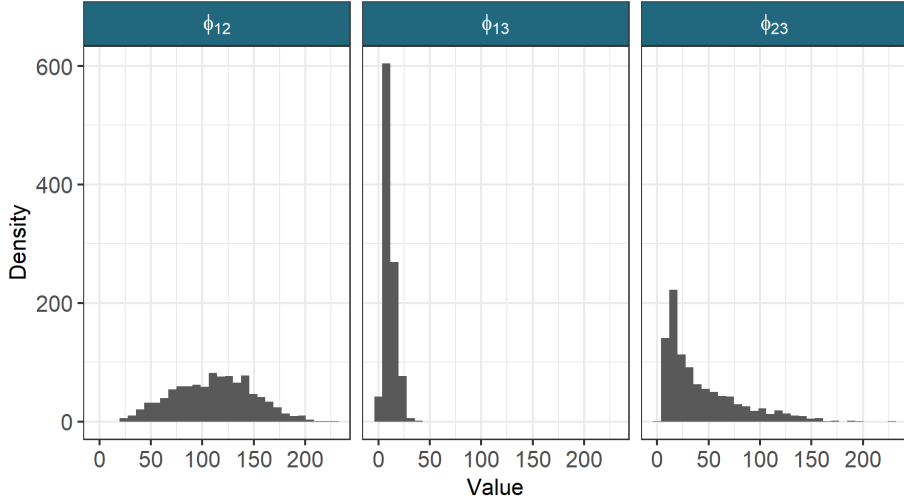


Figure 16: The sampled values for the  $\phi$  parameters from the learners constituting the ensemble. High values indicate similar structure, low values indicate less, with 0 implying that the clustering models on each dataset are independent. The Timecourse dataset is represented by an index of 1, ChIP-chip by 2 and the PPI data by 3.

- Timecourse + PPI: 12 (68),
- ChIP-chip + PPI: 43 (99). .

which aligns with the sampled  $\phi_{lm}$  values in figure 16, which shows that the Timecourse and ChIP-chip datasets contain very similar structure, the ChIP-chip and PPI datasets have some similarity but significantly less and the Timecourse and PPI datasets have less similarity again.

Compare this to the original analysis of this data in Kirk et al. (2012), where the number of integrated genes in each combination is:

- Timecourse + ChIP-chip + PPI: 16,
- Timecourse + ChIP-chip: 32 (48),
- Timecourse + PPI: 16 (32),
- ChIP-chip + PPI: 15 (31).

Our analysis has found significantly more shared structure.

### 5.2.2 Timecourse ChIP-chip analysis

We focus upon the dataset pairing of Timecourse + ChIP-chip as the combination with the greatest number of integrated genes. We show the integrated clusters that emerge in figure 17. In this plot we exclude the 15 clusters where more than half of the member genes have no interactions in the ChIP-chip data and any clusters of one. We find that a small number of transcription factors dominate, with different combinations emerging across the 10 clusters shown here in table 2. Many of these 10 correspond to transcription factors that are well known to regulate cell cycle expression, namely MBP1, SWI4, SWI6, MCM1, FKH1, FKH2, NDD1, SWI5, and ACE2 (Simon et al., 2001).

Table 2: Table of transcription factors prominent in integrated clusters for the Timecourse and ChIP-chip datasets.

Gene	Name	Description
YLR131C	ACE2	Transcription factor required for septum destruction after cytokinesis; phosphorylation by Cbk1p blocks nuclear exit during M/G1 transition; phosphorylation by cyclins Cdc28p and Pho85p prevents nuclear import during cell cycle phases other than cytokinesis; part of RAM network that regulates cellular polarity and morphogenesis; ACE2 has a paralog, SWI5, that arose from the whole genome duplication
YPL049C	DIG1	MAP kinase-responsive inhibitor of the Ste12p transcription factor; involved in the regulation of mating-specific genes and the invasive growth pathway; Dig1p and paralog Dig2p bind to Ste12p
YIL131C	FKH1	Forkhead family transcription factor; evolutionarily conserved lifespan regulator; binds multiple chromosomal elements with distinct specificities, cell cycle dynamics; regulates transcription elongation, chromatin silencing at mating loci, expression of G2/M phase genes
YNL068C	FKH2	Forkhead family transcription factor; rate-limiting activator of replication origins; evolutionarily conserved regulator of lifespan; binds multiple chromosomal elements with distinct specificities, cell cycle dynamics; positively regulates transcriptional elongation; negative role in chromatin silencing at HML and HMR; major role in expression of G2/M phase genes
YDL056W	MBP1	Transcription factor; involved in regulation of cell cycle progression from G1 to S phase, forms a complex with Swi6p that binds to MluI cell cycle box regulatory element in promoters of DNA synthesis genes

YMR043W	MCM1	Transcription factor; involved in cell-type-specific transcription and pheromone response; plays a central role in the formation of both repressor and activator complexes; involved in the transcription of some M/G1 genes Simon et al. (2001).
YOR372C	NDD1	Transcriptional activator essential for nuclear division; essential component of the mechanism that activates the expression of a set of late-S-phase-specific genes; turnover is tightly regulated during cell cycle and in response to DNA damage
YHR084W	STE12	Transcription factor that is activated by a MAPK signalling cascade; activates genes involved in mating or pseudohyphal/invasive growth pathways; cooperates with Tec1p transcription factor to regulate genes specific for invasive growth
YER111C	SWI4	DNA binding component of the SBF complex (Swi4p-Swi6p); a transcriptional activator that in concert with MBF (Mbp1p-Swi6p) regulates late G1-specific transcription of targets including cyclins and genes required for DNA synthesis and repair
YDR146C	SWI5	Transcription factor that recruits Mediator and Swi/Snf complexes; activates transcription of genes expressed at the M/G1 phase boundary and in G1 phase; required for expression of the HO gene controlling mating type switching; localization to nucleus occurs during G1 and appears to be regulated by phosphorylation by Cdc28p kinase; SWI5 has a paralog, ACE2, that arose from the whole genome duplication
YLR182W	SWI6	Transcription cofactor; forms complexes with Swi4p (SBF) and Mbp1p (MBF) to regulate transcription at the G1/S transition (Simon et al., 2001); involved in meiotic gene expression; also binds Stb1p to regulate transcription at START; also required for the unfolded protein response, independently of its known transcriptional coactivators
YBR083W	TEC1	Transcription factor targeting filamentation genes and Ty1 expression; Ste12p activation of most filamentation gene promoters depends on Tec1p and Tec1p transcriptional activity is dependent on its association with Ste12p; binds to TCS elements upstream of filamentation genes, which are regulated by Tec1p/Ste12p/Dig1p complex; competes with Dig2p for binding to Ste12p/Dig1p; positive regulator of chronological life span

YML027W	YOX1	Homeobox transcriptional repressor; binds to Mcm1p and to early cell cycle boxes (ECBs) in the promoters of cell cycle-regulated genes expressed in M/G1 phase; phosphorylated by the cyclin Cdc28p; relocates from nucleus to cytoplasm upon DNA replication stress
---------	------	--

These regulatory proteins are found in different combinations across the clusters. Based upon these combinations we associate each cluster with phases of the cell cycle and or some specific processes.

- Cluster 1: both ACE2 and SWI5 emerge. These regulate specific genes at the end of M and early G1 (McBride et al., 1999; Simon et al., 2001).
- Cluster 2: SWI5. This is similar to cluster 1, as ACE2 is a paralog of SWI5; therefore associated with M/G1. Furthermore, inspection of the expression in the timecourse data shows that the members of cluster 2 largely differentiate from those of cluster 1 based upon amplitude, not periodicity, suggesting that these clusters could be merged.
- Cluster 5: MBP1, SWI4 and SWI6. The SBF complex (Swi4p-Swi6p) is a transcriptional activator that in concert with MBF (Mbp1-Swi6p) regulates late G1-specific transcription of targets including cyclins and genes required for DNA synthesis and repair, controlling the transition to S phase (Simon et al., 2001; Iyer et al., 2001; Aligianni et al., 2009).
- Cluster 9: MBP1 and SWI6. These combine to form MBF, which regulates DNA replication and repair (Iyer et al., 2001).
- Cluster 11: DIG1, SWI4, SWI6, and STE12 emerge in all members with some having associations with TEC1. TEC1 and STE12, controls development, including cell adhesion and filament formation and is negatively regulated by DIG1 and DIG2 (van der Felden et al., 2014).
- Cluster 12: MBP1 , SWI4 and SWI6. Similar to cluster 5 in both the Timecourse and ChIP-chip datasets and thus G1/S phase.
- Cluster 16: some MBP1, SWI4 and SWI6. The constituents of this cluster are largely associated with proteins contributing to histones H1, H2A, H2B, H3 and H4, suggesting an S-phase cluster (Ewen, 2000).
- Cluster 17: FKH1 and FKH2. Fkh1p and Fkh2p are required for cell-cycle regulation of transcription during G2/M (Kumar et al., 2000).
- Cluster 20: NDD1 and MCM1 with some FKH2. Mcm1, together with Fkh1 or Fkh2, recruits the Ndd1 protein in late G2, and thus controls the transcription of G2/M genes (Simon et al., 2001; Koranda et al., 2000).

- Cluster 26: YOX1 and MCM1. YOX1 binds to Mcm1p and to early cell cycle boxes (ECBs) in the promoters of cell cycle-regulated genes expressed in M/G1 phase (Pramila et al., 2002).

### 5.2.3 Example analysis - clusters 9 and 16

We briefly analyse clusters 9 and 16 in greater depth. We used the `org.Sc.sgd.db` package to find gene descriptions which are included in table 3. Cluster 9 has strong association with MBP1 and some interactions with SWI6 in figure 17. The Mbp1-Swi6p complex, MBF, is associated with DNA replication (Iyer et al., 2001). In table 3 it can be seen that many of the genes are S-phase and specifically associated with DNA replication, repair and/or recombination. We see several genes that control the replication checkpoint, TOF1, MRC1 and RAD53 emerge (Bando et al., 2009; Lao et al., 2018).

IRR1 is sometimes named SCC3 (Tóth et al., 1999). It forms the complex cohesin, containing Smc1p, Smc3p, Scc1p, and Scc3p, which is required for sister chromatid cohesion in mitotic cells (Klein et al., 1999). Sister chromatid cohesion is established during S-phase (Tóth et al., 1999). Cohesin has many other roles, including transcription regulation, DNA repair, chromosome condensation, homolog pairing (Mehta et al., 2013).

Cluster 16 consists of genes whose products form the histones H1, H2A, H2B, H3 and H4 and then three others, GAS3, NRM1 and PDS1. Histones are the chief protein components of chromatin (Fischle et al., 2003) and are important contributors to gene regulation (Bannister and Kouzarides, 2011). NRM1 is transcriptional co-repressor of MBF-regulated gene expression acting at the transition from G1 to S phase (de Bruin et al., 2006; Aligiani et al., 2009). NRM1 is phosphorylated in response to DNA replication stress, promoting its disassociation from MBF (De Bruin et al., 2008).

PDS1 is an important regulator of anaphase both for the Anaphase Promoting Complex and checkpoint pathways (Yamamoto et al., 1996; Wang et al., 2001) and is required for metaphase I-anaphase I transition (Cooper et al., 2009). An ESP1/PDS1 complex regulates loss of sister chromatid cohesion at the metaphase to anaphase transition in yeast (Ciosk et al., 1998). Pds1p binds to and inhibits the Esp1 class of sister separating proteins, preventing sister chromatids separation before M phase (Ciosk et al., 1998; Tóth et al., 1999).

GAS3 is a poorly understood gene that interacts with both FKH1 and FKH2 in the ChIP-chip dataset. Their products, Fkh1p and Fkh2p, are required for cell-cycle regulation of transcription during G2/M (Kumar et al., 2000). FKH1 is involved in remodelling chromatin during G2/M and FKH2 has negative role in chromatin silencing at HML and HMR. GAS3 also interacts with SMT3 which regulates chromatid cohesion, chromosome segregation, APC-mediated proteolysis, DNA replication and septin ring dynamics. Chromatid cohesion ensures the faithful segregation of chromosomes in mitosis and in both meiotic divisions (Cooper et al., 2009). These previously reported associations and the other members of cluster 16 suggest that GAS3 might have links to chromatin

Consensus clustering  
Fused clusters across Timecourse and ChIP-chip datasets

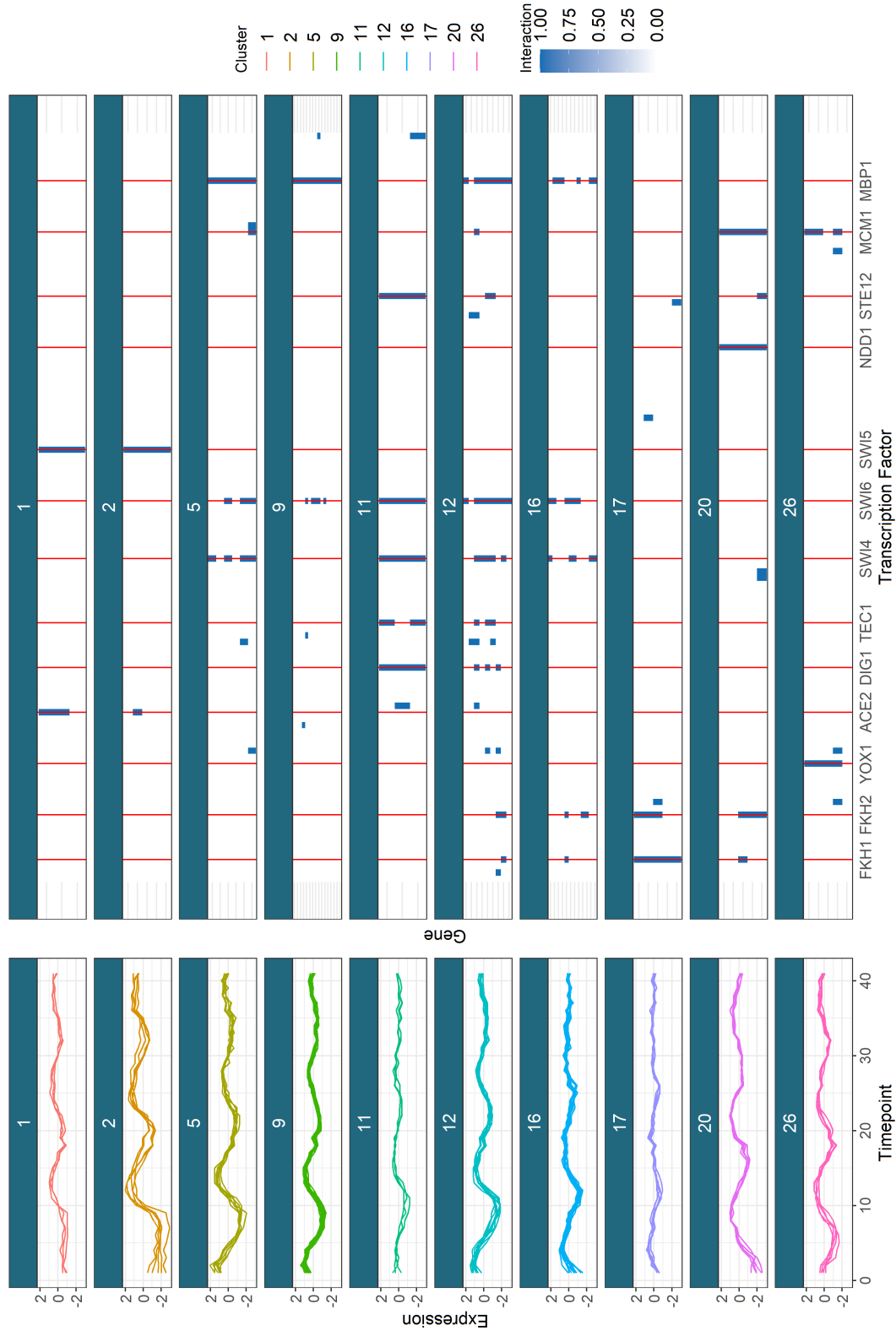


Figure 17: The integrated clusters across the Timecourse and ChIP-chip datasets (as described in table 2?). We exclude the clusters with no interactions in the ChIP-chip dataset and include a red line for the Transcription factors that dominate the clustering structure in the ChIP-chip dataset.

cohesion.

Gene	Name	Cluster	Description
YJL115W	ASF1	9	Nucleosome assembly factor; involved in chromatin assembly, disassembly; required for buffering mRNA synthesis rate against gene dosage changes in S phase
YLR103C	CDC45	9	DNA replication initiation factor; recruited to MCM pre-RC complexes at replication origins; recruits elongation machinery; binds tightly to ssDNA, which disrupts interaction with the MCM helicase and stalls it during replication stress; mutants in human homolog may cause velocardiofacial and DiGeorge syndromes
YPL241C	CIN2	9	GTPase-activating protein (GAP) for Cin4p; tubulin folding factor C involved in beta-tubulin (Tub2p) folding; mutants display increased chromosome loss and benomyl sensitivity; human homolog RP2 complements yeast null mutant
YPR175W	DPB2	9	Second largest subunit of DNA polymerase II (DNA polymerase epsilon); required for maintenance of fidelity of chromosomal replication; essential motif in C-terminus is required for formation of the four-subunit Pol epsilon; expression peaks at the G1/S phase boundary; Cdc28p substrate
YIL026C	IRR1	9	Subunit of the cohesin complex; which is required for sister chromatid cohesion during mitosis and meiosis and interacts with centromeres and chromosome arms
YCL061C	MRC1	9	S-phase checkpoint protein required for DNA replication; couples DNA helicase and polymerase; defines a novel S-phase checkpoint with Hog1p that coordinates DNA replication and transcription upon osmostress; protects uncapped telomeres; Dia2p-dependent degradation mediates checkpoint recovery; mammalian claspin homolog; subunit of a replication-pausing checkpoint complex, Tof1p-Mrc1p-Csm3p; checkpoint-mediator protein that functions during DNA replication and activates the effector kinase Rad53 (Bando et al., 2009); human ATR homolog (Lao et al., 2018)
YDR097C	MSH6	9	Protein required for mismatch repair in mitosis and meiosis; forms a complex with Msh2p to repair both single-base and insertion-deletion mispairs; also involved in interstrand cross-link repair; potentially phosphorylated by Cdc28p

YNL102W	POL1	9	Catalytic subunit of the DNA polymerase I alpha-prime complex; required for the initiation of DNA replication during mitotic DNA synthesis and premeiotic DNA synthesis
YBL035C	POL12	9	B subunit of DNA polymerase alpha-prime complex; required for initiation of DNA replication during mitotic and premeiotic DNA synthesis; also functions in telomere capping and length regulation
YKL113C	RAD27	9	5' to 3' exonuclease, 5' flap endonuclease; required for Okazaki fragment processing and maturation, for long-patch base-excision repair and large loop repair (LLR), ribonucleotide excision repair
YPL153C	RAD53	9	DNA damage response protein kinase; required for cell-cycle arrest, regulation of copper genes in response to DNA damage; human homolog CHEK2 implicated in breast cancer can complement yeast null mutant
YAR007C	RFA1	9	Subunit of heterotrimeric Replication Protein A (RPA); RPA is a highly conserved single-stranded DNA binding protein involved in DNA replication, repair, and recombination; RPA protects against inappropriate telomere recombination, and upon telomere uncapping, prevents cell proliferation by a checkpoint-independent pathway; role in DNA catenation/decatenation pathway of chromosome disentangling; relocates to the cytosol in response to hypoxia
YNL312W	RFA2	9	Subunit of heterotrimeric Replication Protein A (RPA); RPA is a highly conserved single-stranded DNA binding protein involved in DNA replication, repair, and recombination; RPA protects against inappropriate telomere recombination, and upon telomere uncapping, prevents cell proliferation by a checkpoint-independent pathway; in concert with Sgs1p-Top2p-Rmi1p, stimulates DNA catenation/decatenation activity of Top3p; protein abundance increases in response to DNA replication
YAR008W	SEN34	9	s Subunit of the tRNA splicing endonuclease; tRNA splicing endonuclease (Sen complex) is composed of Sen2p, Sen15p, Sen34p, and Sen54p; Sen complex also cleaves the CBP1 mRNA at the mitochondrial surface; Sen34p contains the active site for tRNA 3' splice site cleavage and has similarity to Sen2p and to Archaeal tRNA splicing endonuclease

YJL074C	SMC3	9	Subunit of the multiprotein cohesin complex; required for sister chromatid cohesion in mitotic cells; also required, with Rec8p, for cohesion and recombination during meiosis; phylogenetically conserved SMC chromosomal ATPase family member
YNL273W	TOF1	9	Subunit of a replication-pausing checkpoint complex; Tof1p-Mrc1p-Csm3p acts at the stalled replication fork to promote sister chromatid cohesion after DNA damage, facilitating gap repair of damaged DNA; interacts with the MCM helicase; checkpoint-mediator protein that functions during DNA replication and activates the effector kinase RAD53 (Bando et al., 2009); human ATM homolog (Lao et al., 2018)
YMR215W	GAS3	16	Putative 1,3-beta-glucanosyltransferase; has similarity to other GAS family members; low abundance, possibly inactive member of the GAS family of GPI-containing proteins; localizes to the cell wall; mRNA induced during sporulation
YBR009C	HHF1	16	Histone H4; core histone protein required for chromatin assembly and chromosome function; one of two identical histone proteins (see also HHF2); contributes to telomeric silencing; N-terminal domain involved in maintaining genomic integrity
YNL030W	HHF2	16	Histone H4; core histone protein required for chromatin assembly and chromosome function; one of two identical histone proteins (see also HHF1); contributes to telomeric silencing; N-terminal domain involved in maintaining genomic integrity
YPL127C	HHO1	16	Histone H1, linker histone with roles in meiosis and sporulation; decreasing levels early in sporulation may promote meiosis, and increasing levels during sporulation facilitate compaction of spore chromatin; binds to promoters and within genes in mature spores; may be recruited by Ume6p to promoter regions, contributing to transcriptional repression outside of meiosis; suppresses DNA repair involving homologous recombination
YBR010W	HHT1	16	Histone H3; core histone protein required for chromatin assembly, part of heterochromatin-mediated telomeric and HM silencing; one of two identical histone H3 proteins (see HHT2); regulated by acetylation, methylation, and phosphorylation; H3K14 acetylation plays an important role in the unfolding of strongly positioned nucleosomes during repair of UV damage

YNL031C	HHT2	16	Histone H3; core histone protein required for chromatin assembly, part of heterochromatin-mediated telomeric and HM silencing; one of two identical histone H3 proteins (see HHT1); regulated by acetylation, methylation, and phosphorylation; H3K14 acetylation plays an important role in the unfolding of strongly positioned nucleosomes during repair of UV damage
YDR225W	HTA1	16	Histone H2A; core histone protein required for chromatin assembly and chromosome function; one of two nearly identical subtypes (see also HTA2); DNA damage-dependent phosphorylation by Mec1p facilitates DNA repair; acetylated by Nat4p; N-terminally propionylated <i>in vivo</i>
YBL003C	HTA2	16	Histone H2A; core histone protein required for chromatin assembly and chromosome function; one of two nearly identical (see also HTA1) subtypes; DNA damage-dependent phosphorylation by Mec1p facilitates DNA repair; acetylated by Nat4p
YDR224C	HTB1	16	Histone H2B; core histone protein required for chromatin assembly and chromosome function; nearly identical to HTB2; Rad6p-Bre1p-Lge1p mediated ubiquitination regulates reassembly after DNA replication, transcriptional activation, meiotic DSB formation and H3 methylation
YBL002W	HTB2	16	Histone H2B; core histone protein required for chromatin assembly and chromosome function; nearly identical to HTB1; Rad6p-Bre1p-Lge1p mediated ubiquitination regulates reassembly after DNA replication, transcriptional activation, meiotic DSB formation and H3 methylation
YNR009W	NRM1	16	Transcriptional co-repressor of MBF-regulated gene expression; Nrm1p associates stably with promoters via MCB binding factor (MBF) to repress transcription upon exit from G1 phase
YDR113C	PDS1	16	Securin; inhibits anaphase by binding separin Esp1p; blocks cyclin destruction and mitotic exit, essential for meiotic progression and mitotic cell cycle arrest; localization is cell-cycle dependent and regulated by Cdc28p phosphorylation

Table 3: Integrated genes for the Timecourse and ChIP-chip datasets from clusters 9 and 16.

## Timecourse

Consensus matrices

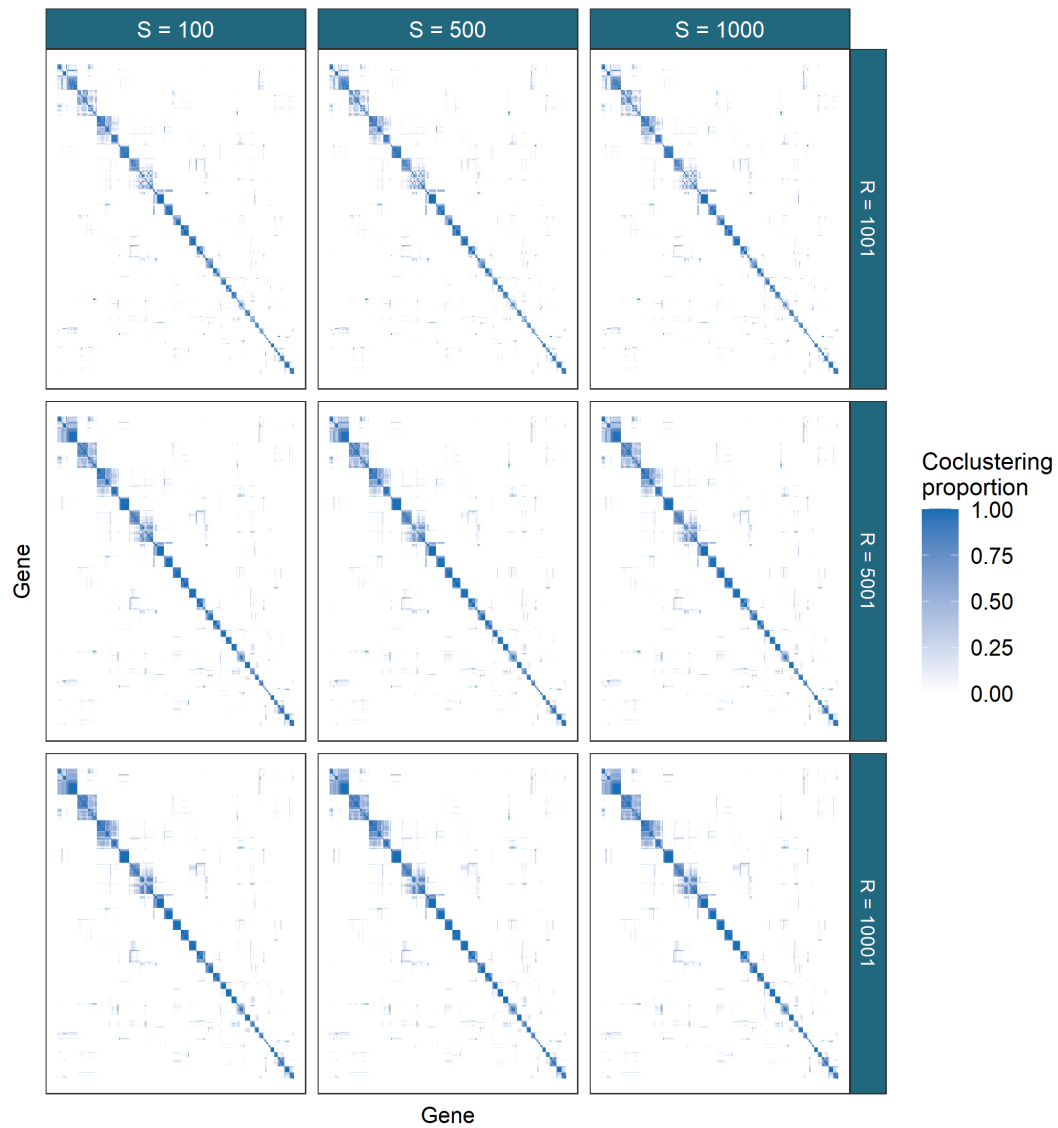


Figure 18: Consensus matrices for different ensembles of MDI for the Timecourse data. This dataset has stable clustering across the different choices of number of chains,  $S$ , and chain depth,  $R$ , with some components merging as the chain depth increases.

## ChIP-chip

### Consensus matrices

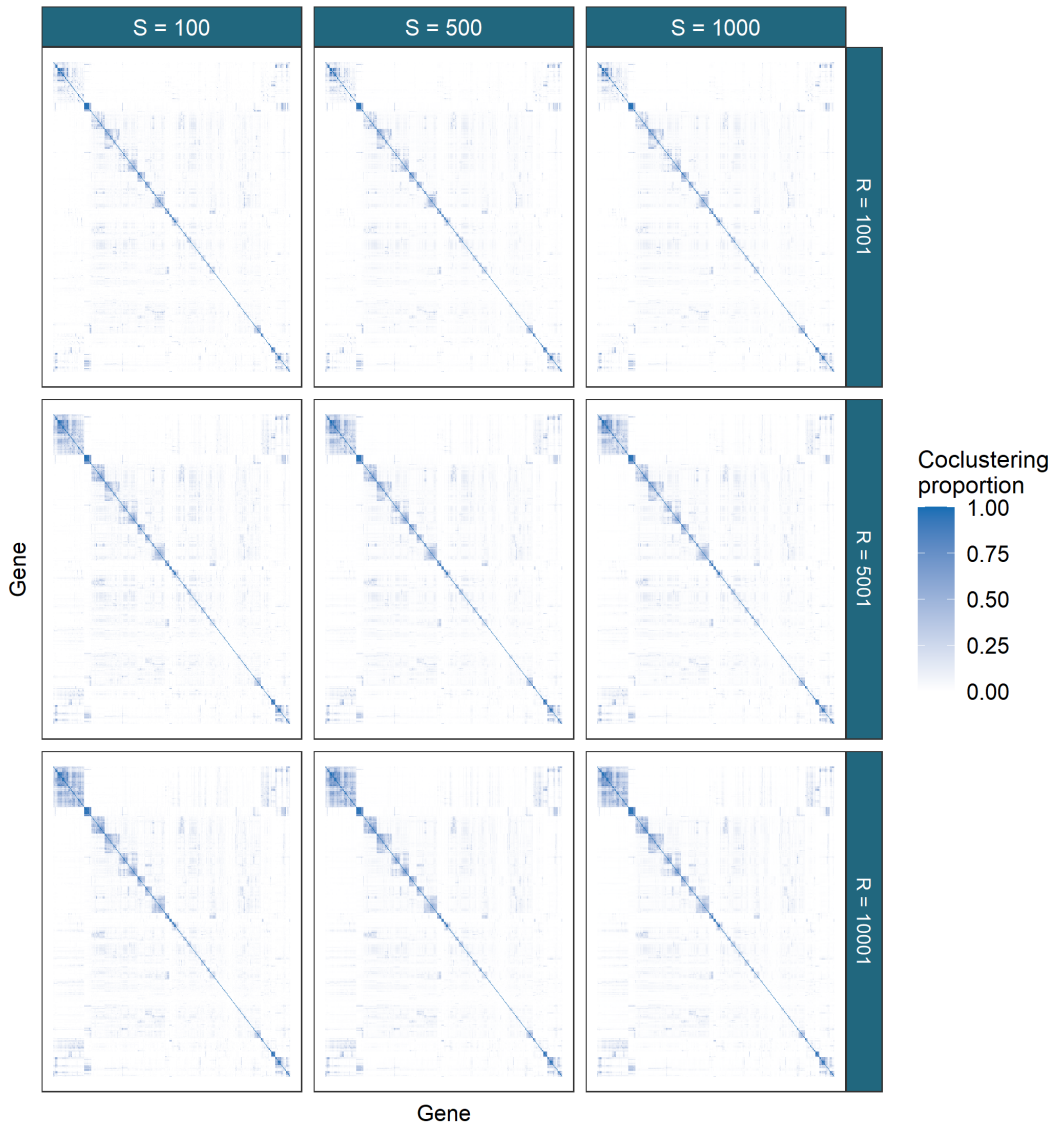


Figure 19: The ChIP-chip dataset is more sparse than the Timecourse data. In keeping with the results from the simulations for mixture models, deeper chains are required for better performance. It is only between  $R = 5,001$  and  $R = 10,001$  that no change in the clustering can be observed and the result is believed to be stable. In this dataset the number of chains used,  $S$ , appears relatively unimportant, with similar results for  $S = 100, 500, 1000$ .

# PPI

## Consensus matrices

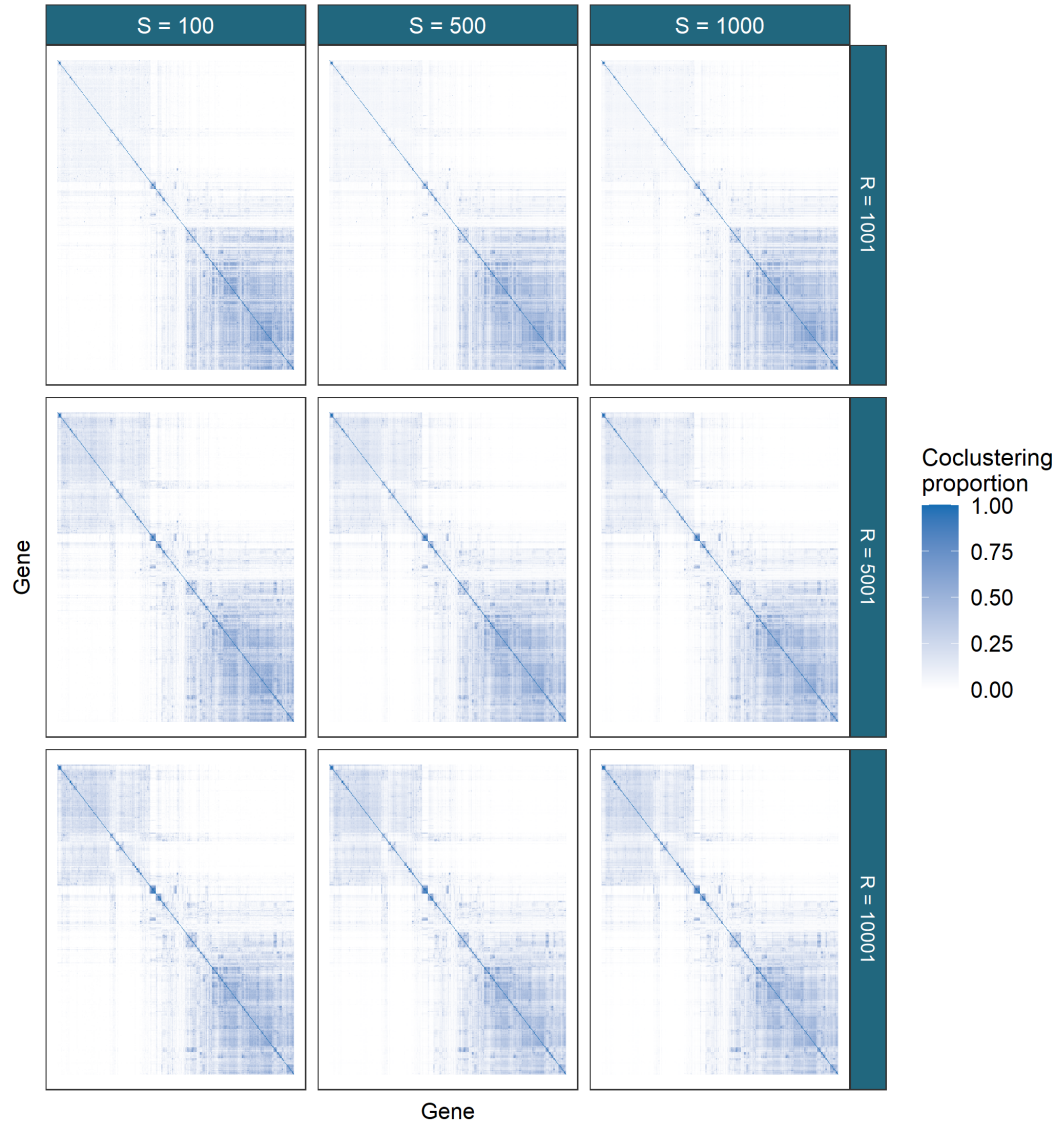


Figure 20: The PPI dataset has awkward characteristics for modelling. A wide, sparse dataset it is chain depth that we found to be the most important parameter for the ensemble. Similar to the results in figure 19, the matrices only stabilise from  $R = 5001$  to  $R = 10001$ .

### 5.3 Bayesian analysis

We wished to compare our results from Consensus clustering to a conventional Bayesian approach. We ran 10 chains of MDI for 36 hours saving every thousandth sample. This resulted in chains of varying length. We reduced the chains to 666 samples as this was the number of samples achieved by the slowest chain. Similar to section 4.1 these chains were then investigated for

- within-chain stationarity using the Geweke convergence diagnostic (Geweke et al., 1991), and
- across-chain convergence using  $\hat{R}$  (Gelman et al., 1992) and the Vats-Knudson extension (*stable*  $\hat{R}$ , Vats and Knudson, 2018).

Again we focus upon stationarity of the continuous variables. In the implementation of MDI we used, the recorded continuous variables are the concentration parameters of the Dirichlet distribution for the dataset-specific component weights and the  $\phi_{ij}$  parameter associated with the correlation between the  $i^{th}$  and  $j^{th}$  datasets.

We plot the Geweke-statistic for each chain in figure 21. No chain is perfectly behaved; as we cannot reduce to the set of stationary chains we thus exclude the **most** poorly behaved chains. Our lack of belief in the convergence of these chains is fortified by the behaviour of  $\hat{R}$  (which can be seen in figure 22) and the different distributions sampled for the  $\phi_{lm}$  parameters shown in figure 23.

We visualise the PSMs for each dataset in figure 24.

If we compare the distribution of sampled values for the  $\phi$  parameters for the Bayesian chains that we keep based upon their convergence diagnostics, the final ensemble used ( $R = 10001$ ,  $S = 1000$ ) and the pooled samples from the 5 long chains, then we see that the ensemble consisting of the long chains (which might be believed to sampling different parts of the posterior distribution) is closer in its appearance to the distributions sampled by the Consensus clustering than to any single chain. There is no consistent distribution across the chains; this lack of agreement leaves us uncomfortable proceeding with the Bayesian analysis. Choosing the result of any single chain over the others feels arbitrary. If we instead pool the samples, which might be a reasonable compromise, it appears that the final distribution is more similar to Consensus clustering than any single chain. In this case it appears that Consensus clustering is more likely to provide a reproducible analysis.

### 5.4 GO term over-representation

We show this lack of disagreement between chains in a Gene Ontology (GO) term over-representation analysis. We estimated clusterings from the PSMs of the chains kept from section 5.3 visualised in figure 24 and the Consensus matrix of the largest ensemble run (i.e.  $CC(10001, 1000)$ ) using the `maxpear` function from the R package `mcclust` Fritsch (2012) using default settings except for `k.max` which was set to  $275 \approx N/2$ . To perform the GO term over-representation analysis we used the Bioconductor packages `clusterProfiler`

## Within chain convergence

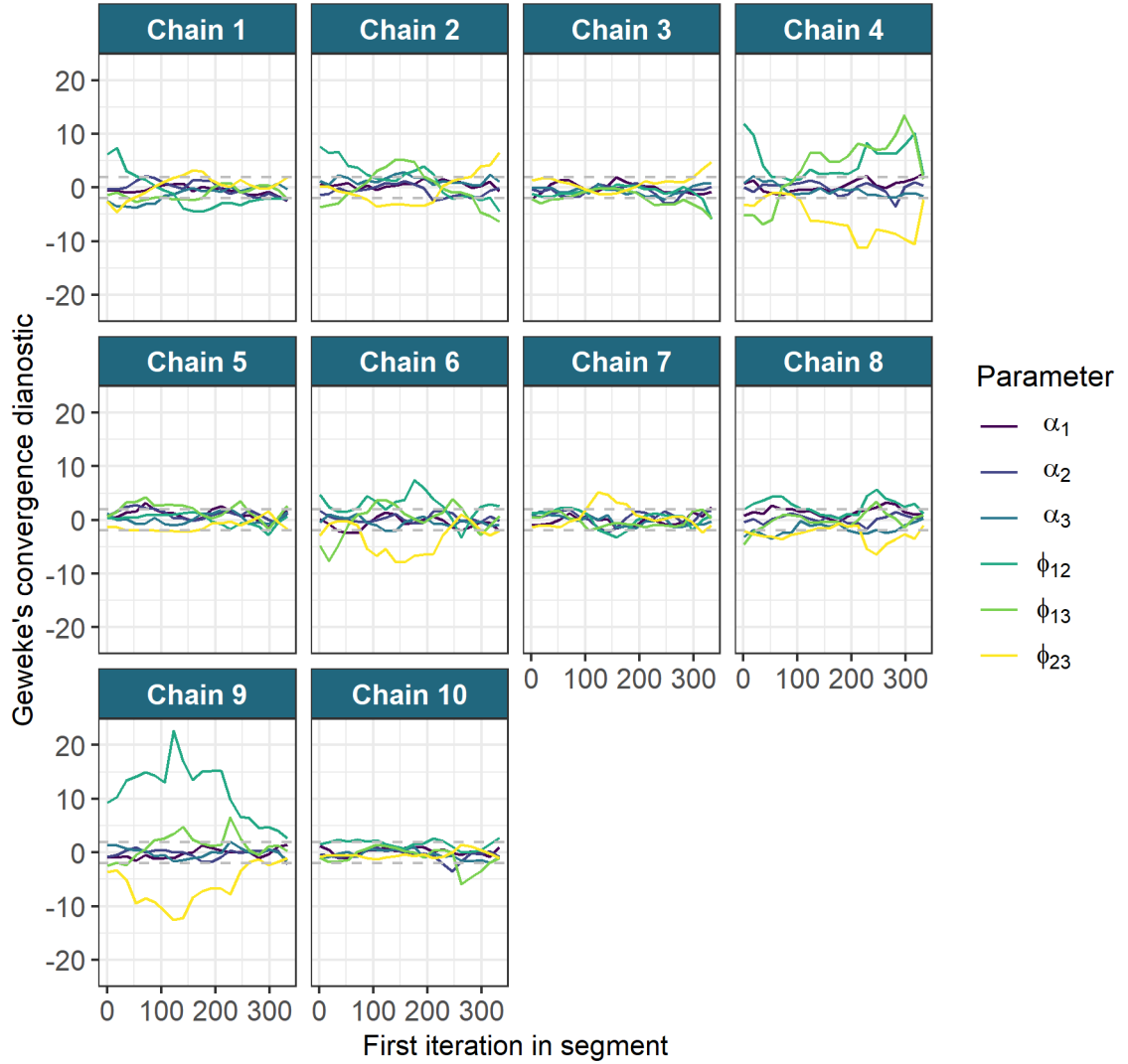


Figure 21: Chain 9 can be seen to have the most extreme behaviour in the distribution of the Geweke diagnostic for the parameters. We remove this chain from the analysis. Of the remaining chains we believe that 1, 2, 4 and 6 express the distributions furthest removed from the desired behaviour and are dropped from the analysis.

## Gelman-R Rubin diagnostic plot

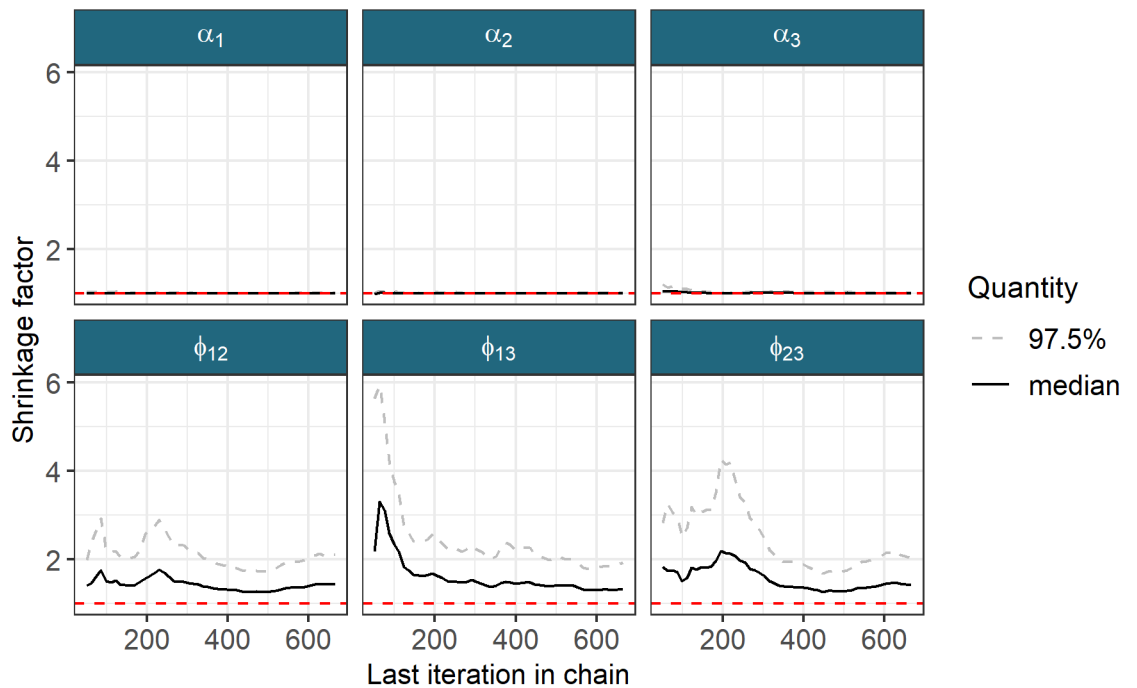


Figure 22: The chains still appear to be unconverged with  $\hat{R}$  remaining above 1.25 for the  $\phi_{12}, \phi_{13}$  and  $\phi_{23}$  parameters. Stable  $\hat{R}$  is also too high with values of 1.049, 1.052 and 1.057 for  $\phi_{12}, \phi_{13}$  and  $\phi_{23}$  respectively.

## Parameter density

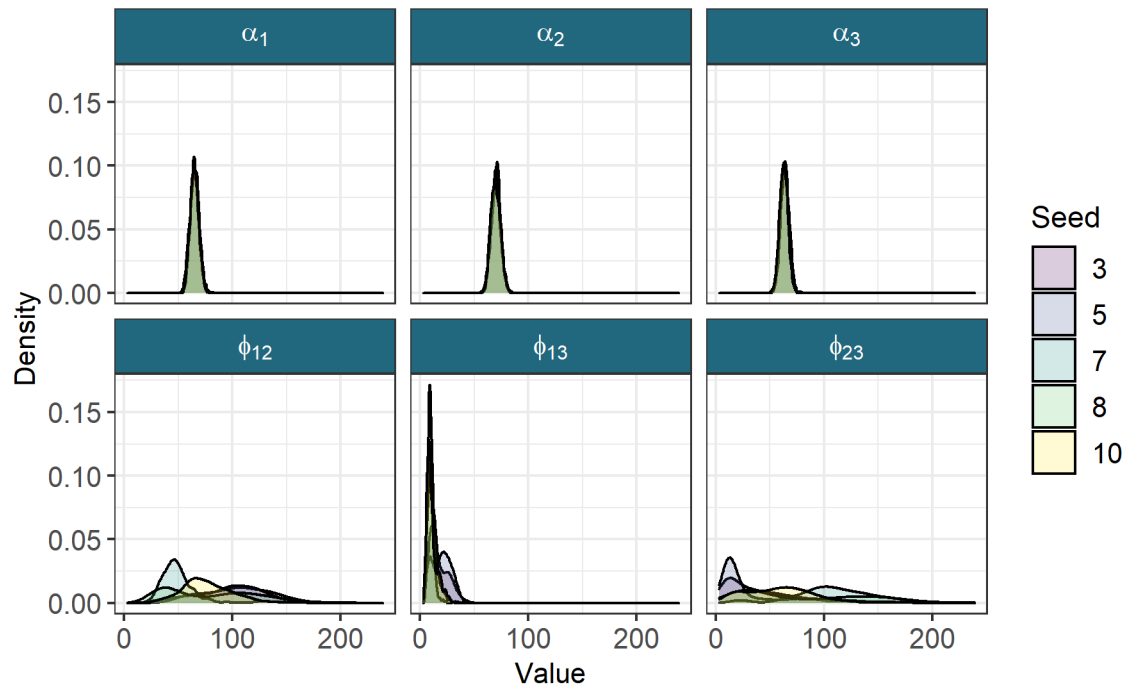


Figure 23: The densities of the continuous variables across the 5 chains kept for analysis. The mean sampled values are  $\alpha_1 = 64.84$ ,  $\alpha_2 = 69.85$ ,  $\alpha_3 = 63.22$ ,  $\phi_{12} = 81.76$ ,  $\phi_{13} = 13.87$ , and  $\phi_{23} = 65.03$ . It can be seen that different modes are being sampled for the  $\phi$  parameters in each chain.

## Yeast dataset

### Posterior similarity matrices

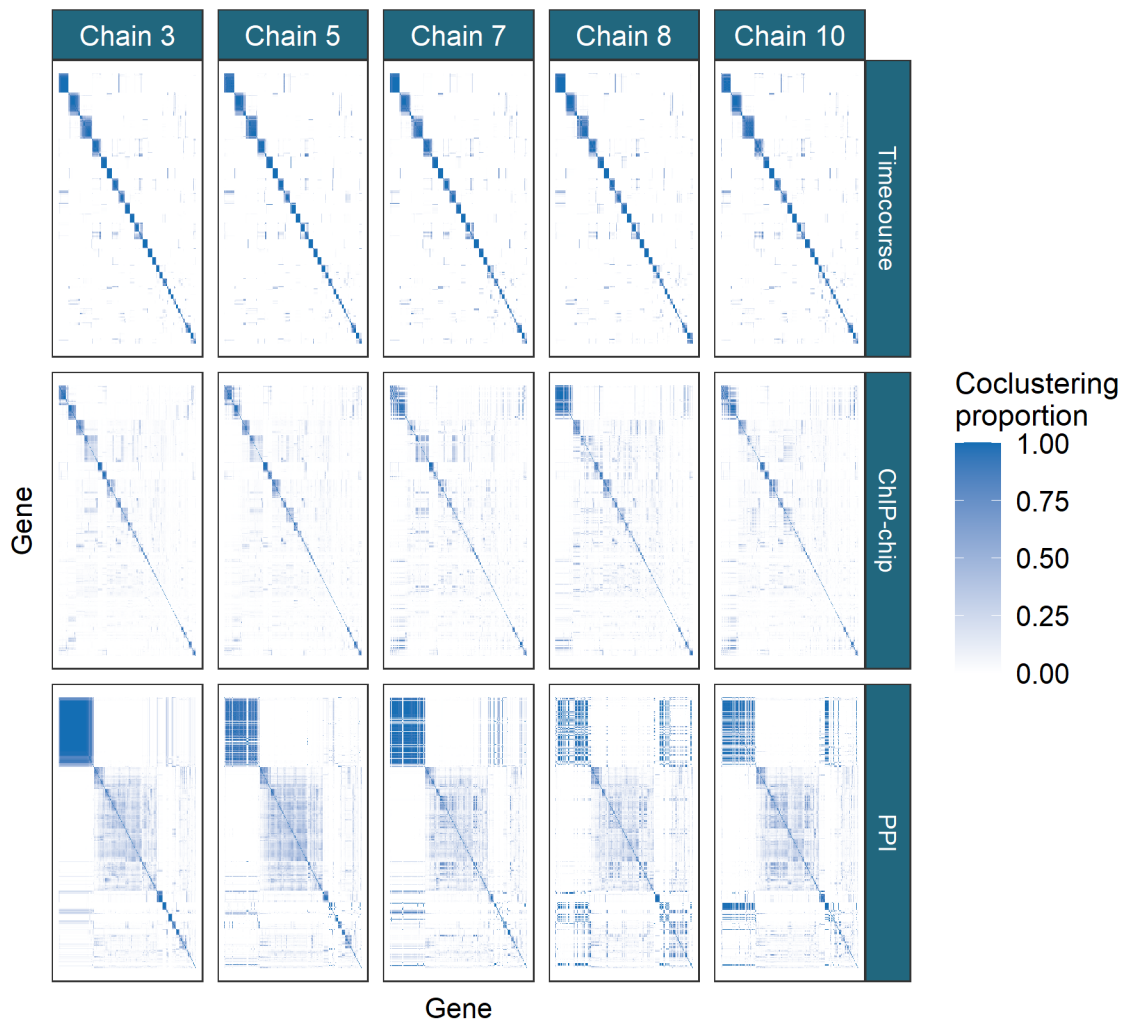


Figure 24: PSMs for each chain within each dataset. The PSMs are ordered by hierarchical clustering of the rows of the PSM for chain 3 in each dataset. There is no marked difference between the matrices for the Timecourse data with disagreement becoming more prominent in the ChIP-chip data and more so again in the PPI dataset.

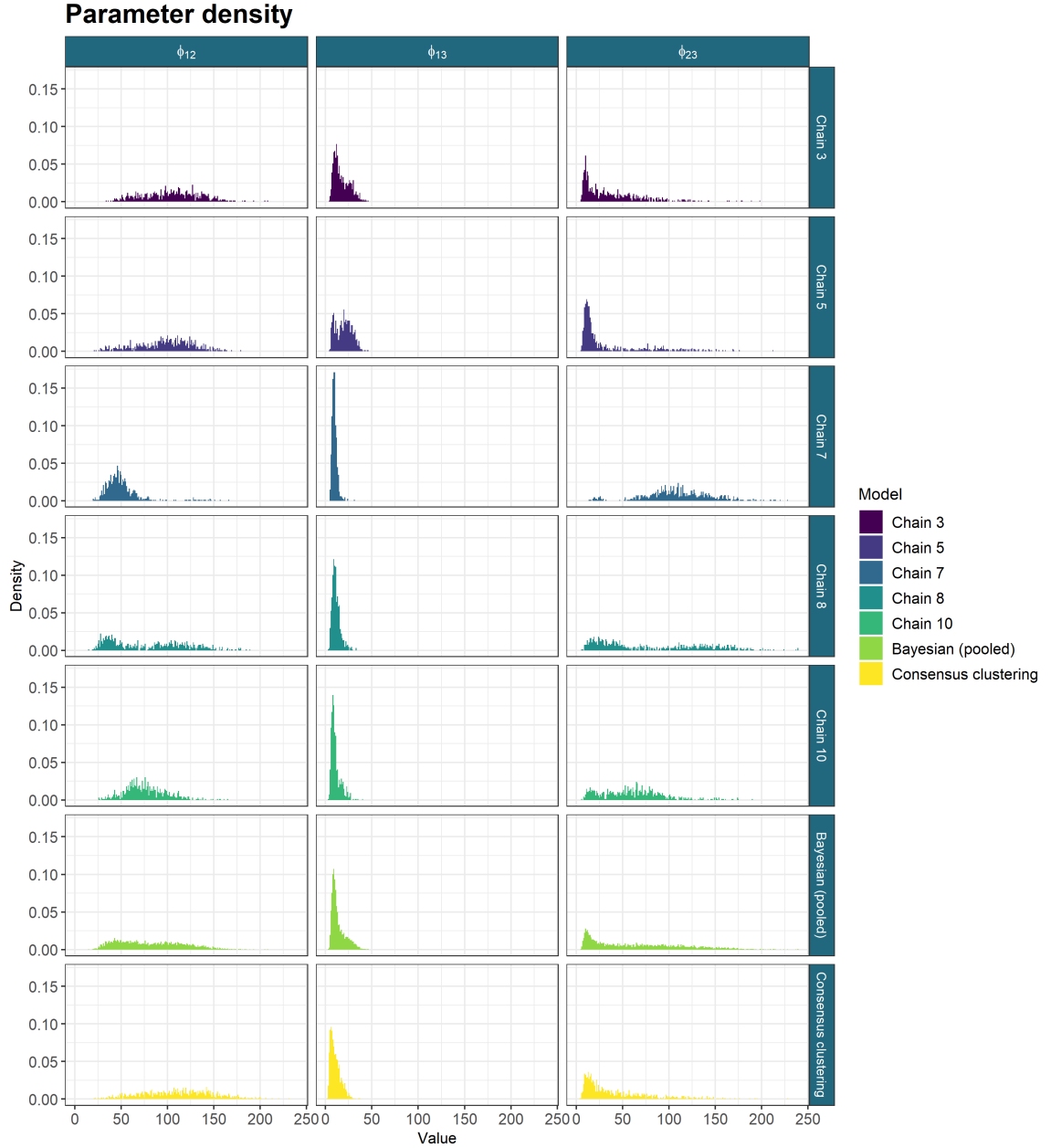


Figure 25: The sampled values for the  $\phi$  parameters from the long chains, their pooled samples and the consensus using 1000 chains of depth 10,001. The long chains display a variety of behaviours. Across chains there is no clear consensus on the nature of the posterior distribution. The samples from any single chain are not particularly close to the behaviour of the pooled samples across all three parameters. It is the Consensus clustering that most approaches this pooled behaviour.

(Yu et al., 2012), **biomaRt** (Durinck et al., 2009) and the annotation package **org.Sc.sgd.db** (Carlson et al., 2014).

We conditioned the test on the background set of the 551 yeast genes in the data. The gene labelled YIL167W was not found in the annotation database and was dropped from the analysis leaving a background universe of 550 genes. A hypergeometric test was used to check if the number of genes associated with specific GO terms within a cluster was greater than expected by random chance. We corrected the  $p$ -values using the Benjamini-Hochberg correction (Benjamini and Hochberg, 1995) and defined significance by a threshold of 0.01. We plotted the over-represented GO terms for the different clusterings within each dataset using the three different ontologies of “Molecular function” (**MF**), “Biological process” (**BP**) and “Cellular component” (**CC**) (figures 26, 27 and 28 respectively).

As we expect based upon the disagreement shown in figure 25, we find that the Bayesian chains have very significant disagreements between each other; there is no consensus on the results with many terms enriched in one or two chains. However, the Consensus clustering finds many of the terms common to all of the long chains. This is what we would expect based upon the similarity of the  $\phi_{lm}$  distribution in the ensemble and the pooled long chains. Consensus clustering also finds some terms with low  $p$ -values common to a majority of chains (such as DNA helicase activity in the MF ontology for the Timecourse dataset) and a small number of GO terms unique to itself. These terms that no long chain find are normally related to other terms already over-represented within either the Consensus clustering or a number of the long chains. For example, the transmembrane transporter activity and transporter activity terms uncovered by the ensemble in the Timecourse dataset are related to terms found across 3 of the chains and by Consensus clustering (specifically transferase activity and phosphotransferase).

## 6 Conclusion

We have shown that Consensus clustering can successfully use Bayesian mixture models as the base learner as well as more complex extensions of these models such as MDI. We found that Consensus clustering sidesteps issues with convergence while offering significant gains in computational time, particularly when used in a parallel environment. We provided a heuristic for deciding upon the number and depth of chains required in an analysis. We then applied Consensus clustering in an integrative analysis of Yeast cell cycle data, uncovering meaningful biological structure in an analysis that is not consistently reproducible using single chains.

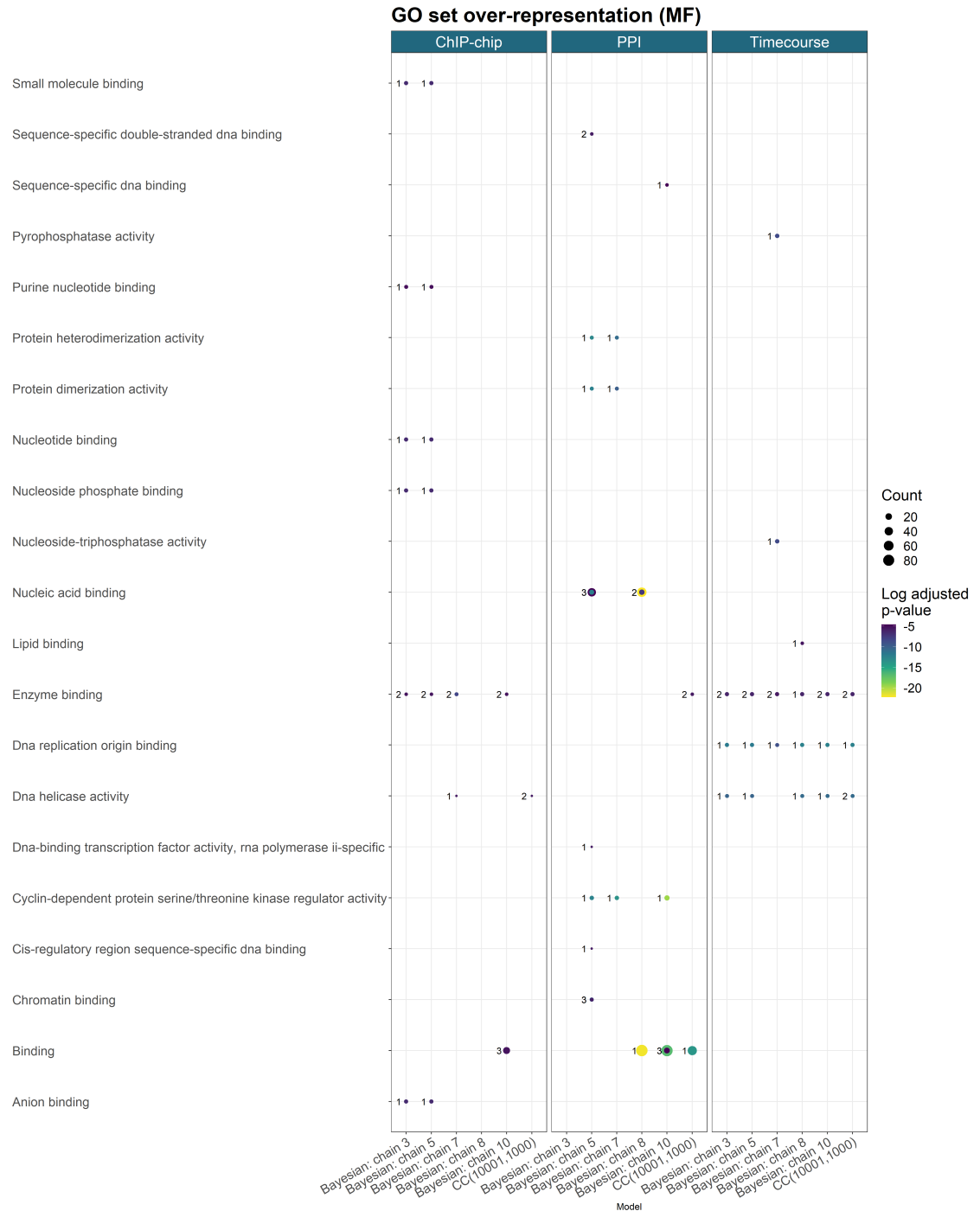


Figure 26: GO term over-representation for the Molecular function ontology for each dataset from the final clustering of each method.

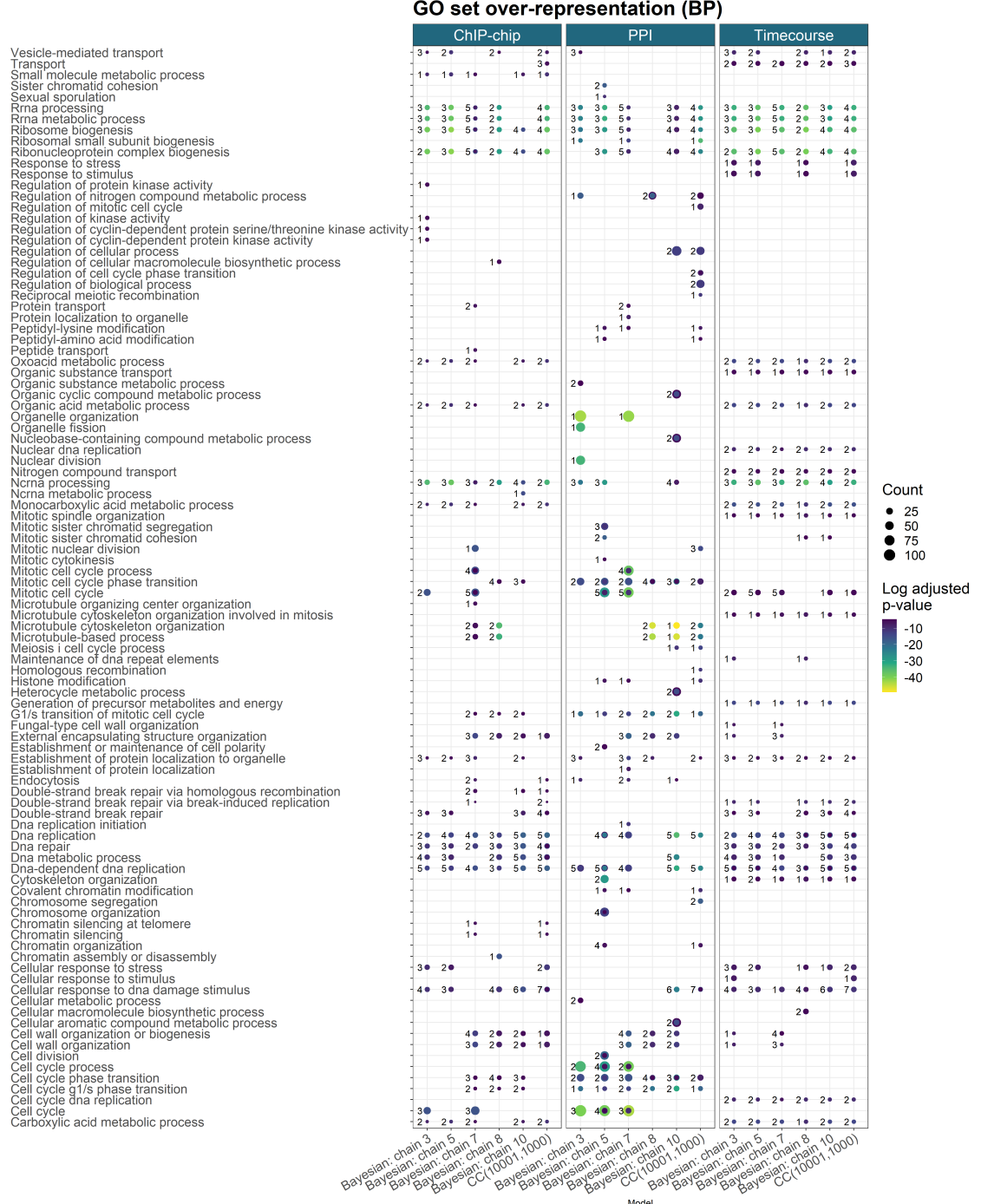


Figure 27: GO term over-representation for the Biological process ontology for each dataset from the final clustering of each method.

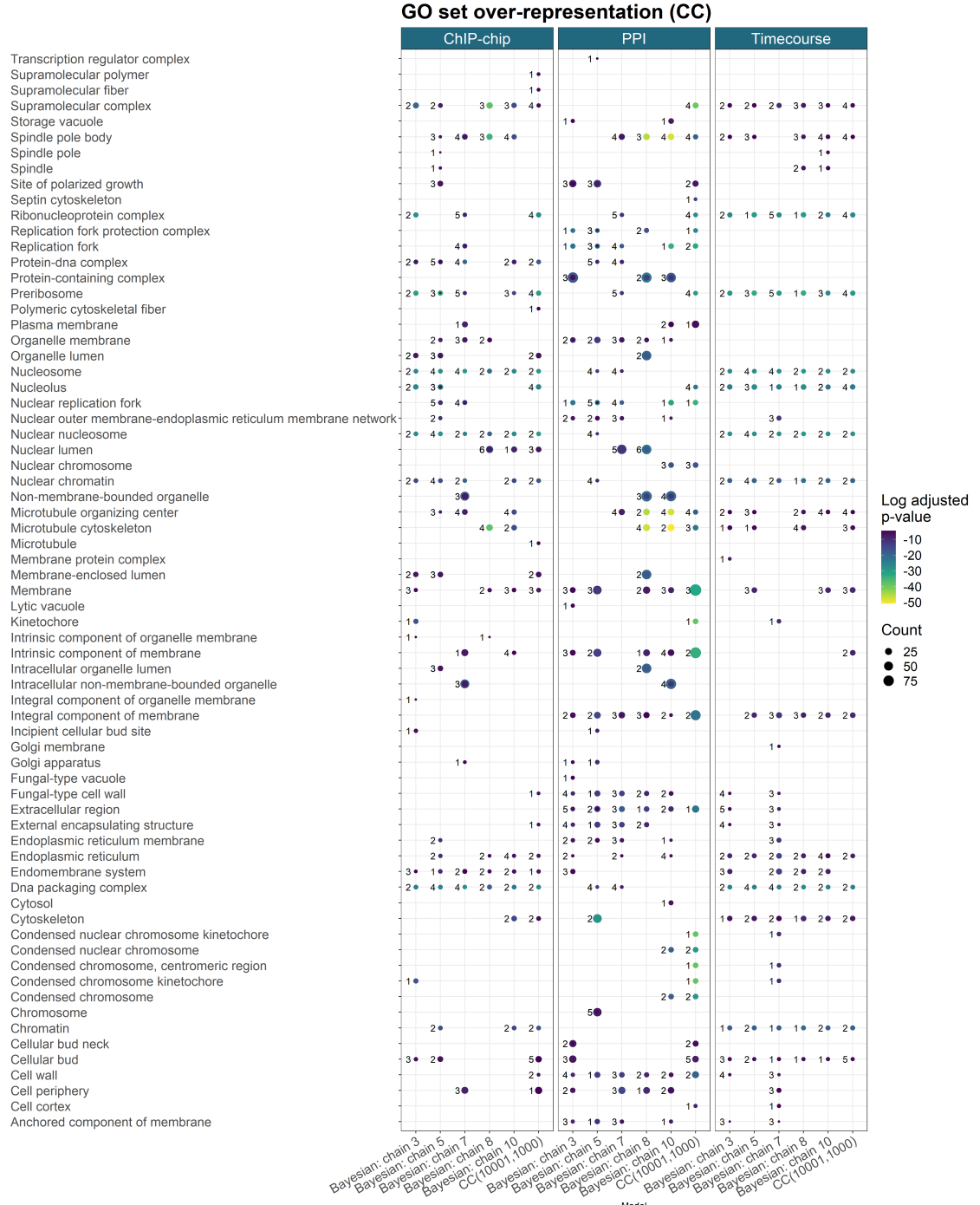


Figure 28: GO term over-representation for the Cellular component ontology for each dataset from the final clustering of each method.

## References

- Bruce Alberts, Alexander Johnson, Julian Lewis, David Morgan, Martin Raff, and Dennis Bray James Watson Keith Roberts, Peter Walter. The cell cycle and programmed cell death. In Werner Dubitzky, Olaf Wolkenhauer, Kwang-Hyun Cho, and Hiroki Yokota, editors, *Molecular biology of the cell*, chapter 17. Garland Science, Taylor and Francis Group, New York, NY, 6 edition, 2018.
- Sofia Aligiani, Daniel H Lackner, Steffi Klier, Gabriella Rustici, Brian T Wilhelm, Samuel Marguerat, Sandra Codlin, Alvis Brazma, Robertus AM de Bruin, and Jürg Bähler. The fission yeast homeodomain protein yox1p binds to mbf and confines mbf-dependent cell-cycle transcription to g1-s via negative feedback. *PLoS Genet*, 5(8):e1000626, 2009.
- Masashige Bando, Yuki Katou, Makiko Komata, Hirokazu Tanaka, Takehiko Itoh, Takashi Sutani, and Katsuhiko Shirahige. Csm3, tof1, and mrc1 form a heterotrimeric mediator complex that associates with dna replication forks. *Journal of Biological Chemistry*, 284(49):34355–34365, 2009.
- Andrew J Bannister and Tony Kouzarides. Regulation of chromatin by histone modifications. *Cell research*, 21(3):381–395, 2011.
- Yoav Benjamini and Yosef Hochberg. Controlling the false discovery rate: a practical and powerful approach to multiple testing. *Journal of the Royal statistical society: series B (Methodological)*, 57(1):289–300, 1995.
- M Carlson, S Falcon, H Pages, and N Li. Org. sc. sgd. db: Genome wide annotation for yeast. *R package version*, 2(1), 2014.
- Katherine C Chen, Laurence Calzone, Attila Csikasz-Nagy, Frederick R Cross, Bela Novak, and John J Tyson. Integrative analysis of cell cycle control in budding yeast. *Molecular biology of the cell*, 15(8):3841–3862, 2004.
- Raymond J Cho, Michael J Campbell, Elizabeth A Winzeler, Lars Steinmetz, Andrew Conway, Lisa Wodicka, Tyra G Wolfsberg, Andrei E Gabrielian, David Landsman, David J Lockhart, et al. A genome-wide transcriptional analysis of the mitotic cell cycle. *Molecular cell*, 2(1):65–73, 1998.
- Rafal Ciosk, Wolfgang Zachariae, Christine Michaelis, Andrej Shevchenko, Matthias Mann, and Kim Nasmyth. An esp1/pds1 complex regulates loss of sister chromatid cohesion at the metaphase to anaphase transition in yeast. *Cell*, 93(6):1067–1076, 1998.
- Katrina F Cooper, Michael J Mallory, Vincent Guacci, Katherine Lowe, and Randy Strich. Pds1p is required for meiotic recombination and prophase i progression in *saccharomyces cerevisiae*. *Genetics*, 181(1):65–79, 2009.

- RAM De Bruin, TI Kalashnikova, A Aslanian, J Wohlschlegel, C Chahwan, JR Yates, P Russell, and C Wittenberg. Dna replication checkpoint promotes g1-s transcription by inactivating the mbf repressor nrm1. *Proceedings of the National Academy of Sciences*, 105(32):11230–11235, 2008.
- Robertus AM de Bruin, Tatyana I Kalashnikova, Charly Chahwan, W Hayes McDonald, James Wohlschlegel, John Yates III, Paul Russell, and Curt Wittenberg. Constraining g1-specific transcription to late g1 phase: the mbf-associated corepressor nrm1 acts via negative feedback. *Molecular cell*, 23(4):483–496, 2006.
- Steffen Durinck, Paul T Spellman, Ewan Birney, and Wolfgang Huber. Mapping identifiers for the integration of genomic datasets with the r/bioconductor package biomart. *Nature protocols*, 4(8):1184, 2009.
- Yasin Şenbabaoğlu, George Michailidis, and Jun Z Li. A reassessment of consensus clustering for class discovery. *bioRxiv*, page 002642, 2014a.
- Yasin Şenbabaoğlu, George Michailidis, and Jun Z Li. Critical limitations of consensus clustering in class discovery. *Scientific reports*, 4(1):1–13, 2014b.
- Mark E Ewen. Where the cell cycle and histones meet. *Genes & development*, 14(18):2265–2270, 2000.
- Wolfgang Fischle, Yanming Wang, and C David Allis. Histone and chromatin cross-talk. *Current opinion in cell biology*, 15(2):172–183, 2003.
- Arno Fritsch. *mcclust: Process an MCMC Sample of Clusterings*, 2012. URL <https://CRAN.R-project.org/package=mcclust>. R package version 1.0.
- Arno Fritsch, Katja Ickstadt, et al. Improved criteria for clustering based on the posterior similarity matrix. *Bayesian analysis*, 4(2):367–391, 2009.
- Evelina Gabasova, John Reid, and Lorenz Wernisch. Clusternomics: Integrative context-dependent clustering for heterogeneous datasets. *PLoS computational biology*, 13(10):e1005781, 2017.
- Andrew Gelman, Donald B Rubin, et al. Inference from iterative simulation using multiple sequences. *Statistical science*, 7(4):457–472, 1992.
- Andrew Gelman, John B Carlin, Hal S Stern, David B Dunson, Aki Vehtari, and Donald B Rubin. *Bayesian data analysis*. CRC press, 2013.
- John Geweke et al. *Evaluating the accuracy of sampling-based approaches to the calculation of posterior moments*, volume 196. Federal Reserve Bank of Minneapolis, Research Department Minneapolis, MN, 1991.
- Reza Ghaemi, Md Nasir Sulaiman, Hamidah Ibrahim, Norwati Mustapha, et al. A survey: clustering ensembles techniques. *World Academy of Science, Engineering and Technology*, 50:636–645, 2009.

- Reza Ghaemi, Nasir bin Sulaiman, Hamidah Ibrahim, and Norwati Mustapha. A review: accuracy optimization in clustering ensembles using genetic algorithms. *Artificial Intelligence Review*, 35(4):287–318, 2011.
- Marina V Granovskaia, Lars J Jensen, Matthew E Ritchie, Joern Toedling, Ye Ning, Peer Bork, Wolfgang Huber, and Lars M Steinmetz. High-resolution transcription atlas of the mitotic cell cycle in budding yeast. *Genome biology*, 11(3):1–11, 2010.
- Christopher T Harbison, D Benjamin Gordon, Tong Ihn Lee, Nicola J Rinaldi, Kenzie D Macisaac, Timothy W Danford, Nancy M Hannett, Jean-Bosco Tagne, David B Reynolds, Jane Yoo, et al. Transcriptional regulatory code of a eukaryotic genome. *Nature*, 431(7004):99–104, 2004.
- BP Ingalls, BP Duncker, DR Kim, and BJ McConkey. Systems level modeling of the cell cycle using budding yeast. *Cancer informatics*, 3: 117693510700300020, 2007.
- Vishwanath R Iyer, Christine E Horak, Charles S Scafe, David Botstein, Michael Snyder, and Patrick O Brown. Genomic binding sites of the yeast cell-cycle transcription factors sbf and mbf. *Nature*, 409(6819):533–538, 2001.
- Javier Jiménez, Samuel Bru, Mariana Ribeiro, and Josep Clotet. Live fast, die soon: cell cycle progression and lifespan in yeast cells. *Microbial Cell*, 2(3): 62, 2015.
- M Angeles Juanes. Methods of synchronization of yeast cells for the analysis of cell cycle progression. In *The Mitotic Exit Network*, pages 19–34. Springer, 2017.
- Paul Kirk, Jim E Griffin, Richard S Savage, Zoubin Ghahramani, and David L Wild. Bayesian correlated clustering to integrate multiple datasets. *Bioinformatics*, 28(24):3290–3297, 2012.
- Vladimir Yu Kiselev, Kristina Kirschner, Michael T Schaub, Tallulah Andrews, Andrew Yiu, Tamir Chandra, Kedar N Natarajan, Wolf Reik, Mauricio Barahona, Anthony R Green, et al. Sc3: consensus clustering of single-cell rna-seq data. *Nature methods*, 14(5):483–486, 2017.
- Franz Klein, Peter Mahr, Marta Galova, Sara BC Buonomo, Christine Michaelis, Knud Nairz, and Kim Nasmyth. A central role for cohesins in sister chromatid cohesion, formation of axial elements, and recombination during yeast meiosis. *Cell*, 98(1):91–103, 1999.
- Christina Knudson and Dootika Vats. *stableGR: A Stable Gelman-Rubin Diagnostic for Markov Chain Monte Carlo*, 2020. URL <https://CRAN.R-project.org/package=stableGR>. R package version 1.0.

- Manfred Koranda, Alexander Schleiffer, Lukas Endler, and Gustav Ammerer. Forkhead-like transcription factors recruit ndd1 to the chromatin of g2/m-specific promoters. *Nature*, 406(6791):94–98, 2000.
- Raman Kumar, David M Reynolds, Andrej Shevchenko, Anna Shevchenko, Sherilyn D Goldstone, and Stephen Dalton. Forkhead transcription factors, fkh1p and fkh2p, collaborate with mcm1p to control transcription required for m-phase. *Current Biology*, 10(15):896–906, 2000.
- Jessica P Lao, Katie M Ulrich, Jeffrey R Johnson, Billy W Newton, Ajay A Vashisht, James A Wohlschlegel, Nevan J Krogan, and David P Toczyski. The yeast dna damage checkpoint kinase rad53 targets the exoribonuclease, xrn1. *G3: Genes, Genomes, Genetics*, 8(12):3931–3944, 2018.
- Brian D Lehmann, Joshua A Bauer, Xi Chen, Melinda E Sanders, A Bapsi Chakravarthy, Yu Shyr, Jennifer A Pietenpol, et al. Identification of human triple-negative breast cancer subtypes and preclinical models for selection of targeted therapies. *The Journal of clinical investigation*, 121(7):2750–2767, 2011.
- Samuel A Mason, Faiz Sayyid, Paul DW Kirk, Colin Starr, and David L Wild. Mdi-gpu: accelerating integrative modelling for genomic-scale data using gpu computing. *Statistical Applications in Genetics and Molecular Biology*, 15(1):83–86, 2016.
- Helen J McBride, Yixin Yu, and David J Stillman. Distinct regions of the swi5 and ace2 transcription factors are required for specific gene activation. *Journal of Biological Chemistry*, 274(30):21029–21036, 1999.
- Gunjan D Mehta, Ravinder Kumar, Sanjeeva Srivastava, and Santanu Kumar Ghosh. Cohesin: functions beyond sister chromatid cohesion. *FEBS letters*, 587(15):2299–2312, 2013.
- Nicolai Meinshausen and Peter Bühlmann. Stability selection. *Journal of the Royal Statistical Society: Series B (Statistical Methodology)*, 72(4):417–473, 2010.
- Stefano Monti, Pablo Tamayo, Jill Mesirov, and Todd Golub. Consensus clustering: a resampling-based method for class discovery and visualization of gene expression microarray data. *Machine learning*, 52(1-2):91–118, 2003.
- Tata Pramila, Shawna Miles, Debraj GuhaThakurta, Dave Jemioło, and Linda L Breeden. Conserved homeodomain proteins interact with mads box protein mcm1 to restrict ecb-dependent transcription to the m/g1 phase of the cell cycle. *Genes & development*, 16(23):3034–3045, 2002.
- Richard S Savage, Zoubin Ghahramani, Jim E Griffin, Bernard J De la Cruz, and David L Wild. Discovering transcriptional modules by bayesian data integration. *Bioinformatics*, 26(12):i158–i167, 2010.

- Gideon Schwarz et al. Estimating the dimension of a model. *The annals of statistics*, 6(2):461–464, 1978.
- Samuel Sanford Shapiro and Martin B Wilk. An analysis of variance test for normality (complete samples). *Biometrika*, 52(3/4):591–611, 1965.
- Itamar Simon, John Barnett, Nancy Hannett, Christopher T Harbison, Nicola J Rinaldi, Thomas L Volkert, John J Wyrick, Julia Zeitlinger, David K Gifford, Tommi S Jaakkola, et al. Serial regulation of transcriptional regulators in the yeast cell cycle. *Cell*, 106(6):697–708, 2001.
- Paul T Spellman, Gavin Sherlock, Michael Q Zhang, Vishwanath R Iyer, Kirk Anders, Michael B Eisen, Patrick O Brown, David Botstein, and Bruce Futcher. Comprehensive identification of cell cycle-regulated genes of the yeast *Saccharomyces cerevisiae* by microarray hybridization. *Molecular biology of the cell*, 9(12):3273–3297, 1998.
- Chris Stark, Bobby-Joe Breitkreutz, Teresa Reguly, Lorrie Boucher, Ashton Breitkreutz, and Mike Tyers. Biogrid: a general repository for interaction datasets. *Nucleic acids research*, 34(suppl\_1):D535–D539, 2006.
- Attila Tóth, Rafal Ciosk, Frank Uhlmann, Marta Galova, Alexander Schleiffer, and Kim Nasmyth. Yeast cohesin complex requires a conserved protein, eco1p (ctf7), to establish cohesion between sister chromatids during dna replication. *Genes & development*, 13(3):320–333, 1999.
- John J. Tyson, Katherine C. Chen, and Béla Novák. Cell cycle, budding yeast. In Werner Dubitzky, Olaf Wolkenhauer, Kwang-Hyun Cho, and Hiroki Yokota, editors, *Encyclopedia of Systems Biology*, pages 337–341. Springer New York, New York, NY, 2013.
- Julia van der Felden, Sarah Weisser, Stefan Brückner, Peter Lenz, and Hans-Ulrich Mösch. The transcription factors tec1 and ste12 interact with coregulators msa1 and msa2 to activate adhesion and multicellular development. *Molecular and cellular biology*, 34(12):2283–2293, 2014.
- Dootika Vats and Christina Knudson. Revisiting the gelman-rubin diagnostic. *arXiv preprint arXiv:1812.09384*, 2018.
- Roel GW Verhaak, Katherine A Hoadley, Elizabeth Purdom, Victoria Wang, Yuan Qi, Matthew D Wilkerson, C Ryan Miller, Li Ding, Todd Golub, Jill P Mesirov, et al. Integrated genomic analysis identifies clinically relevant subtypes of glioblastoma characterized by abnormalities in pdgfra, idh1, egfr, and nf1. *Cancer cell*, 17(1):98–110, 2010.
- Ulrike Von Luxburg and Shai Ben-David. Towards a statistical theory of clustering. In *Pascal workshop on statistics and optimization of clustering*, pages 20–26. Citeseer, 2005.

Hong Wang, Dou Liu, Yanchang Wang, Jun Qin, and Stephen J Elledge. Pds1 phosphorylation in response to dna damage is essential for its dna damage checkpoint function. *Genes & development*, 15(11):1361–1372, 2001.

Wilkerson, Matthew D., Hayes, and D. Neil. Consensusclusterplus: a class discovery tool with confidence assessments and item tracking. *Bioinformatics*, 26(12):1572–1573, 2010.

Jun-Yu Xu, Chunchao Zhang, Xiang Wang, Linhui Zhai, Yiming Ma, Yousheng Mao, Kun Qian, Changqing Sun, Zhiwei Liu, Shangwen Jiang, et al. Integrative proteomic characterization of human lung adenocarcinoma. *Cell*, 182(1):245–261, 2020.

Ayumu Yamamoto, Vincent Guacci, and Douglas Koshland. Pds1p, an inhibitor of anaphase in budding yeast, plays a critical role in the apc and checkpoint pathway (s). *The Journal of cell biology*, 133(1):99–110, 1996.

Guangchuang Yu, Li-Gen Wang, Yanyan Han, and Qing-Yu He. clusterprofiler: an r package for comparing biological themes among gene clusters. *OMICS: A Journal of Integrative Biology*, 16(5):284–287, 2012. doi: 10.1089/omi.2011.0118.